The Pennsylvania State University

The Graduate School

College of Earth and Mineral Science

TESTING THE VIABILITY OF SUPERCRITICAL CARBON DIOXIDE AS A FRACKING FLUID BY COMPUTING ITS CHEMICAL INTERACTION WITH ILLITE

A Thesis in

Geosciences

by

Oluwaseyi Ajayi

Submitted in Partial Fulfillment

of the Requirements

for the Degree of

Master of Science

May 2017

The thesis of Oluwaseyi Ajayi was reviewed and approved* by the following:

Michael Arthur

Professor of Geosciences

Derek Elsworth

Professor of Energy and Mineral Engineering and Geosciences

Demian Saffer

Professor of Geosciences

Associate Head for Graduate Programs and Research in Geosciences

*Signatures are on file in the Graduate School

ABSTRACT

In this study, supercritical CO_2 ($scCO_2$) was investigated as a hydraulic fracturing fluid by modeling the interfacial energy of $scCO_2$ versus water with the common shale mineral illite. The interfacial tensions between supercritical CO_2 ($scCO_2$) and illite and H_2O and illite were measured and compared under conditions relevant to hydraulic fracturing using density functional theory (DFT) methods. Different illite models were used, two with a water monolayer (simulating wet pores) and two with a polymethyl methacrylate (PMMA) monolayer (simulating hydrocarbon-filled pores). Additionally, two of the illite models were charged at the surface with 8 K^+ ions and two of the illite models contained no K^+ ions. The illite surface with the water monolayer charged with $8K^+$ ions is most likely to behave as a real illite surface. The calculated interfacial energy between $scCO_2$ and this illite surface was 0.0144 J/m^2 and between water and illite was 0.0397 J/m^2. The lower interfacial energy between $scCO_2$ and illite suggests that $scCO_2$ would create a better fracturing fluid because it can enter the nanopores of illite-dominated shales more readily than water. The orientations of the $scCO_2$ molecules with respect to the illite also suggest that $scCO_2$ is not influenced by a charged ion surface on the surface of the illite whereas the water is; these surface orientations explain the disparity between the interfacial energies between $scCO_2$ and illite and water and illite.

TABLE OF CONTENTS

LIST OF FIGURES

LIST OF TABLES

ACKNOWLEDGEMENTS

Special acknowledgements go to Mark DelloStritto (Department of Physics-Penn State) for providing codes for analysis of our results and Dr. Randall T. Cygan (Sandia National Laboratory) for providing illite models. I thank the Mildred S. Bunton and Calvin H. Waller Undergraduate Fellows program for providing one year of funding for my graduate research. I also thank Shell for providing another year of funding for my graduate research through the Petroleum Geosystems Initiative.

I thank Jason Boettger, Dr. Michael Arthur, and Dr. Derek Ellsworth (Department of Geosciences-Penn State) for assisting with their expertise, giving me better background knowledge to research effectively. Finally, I would like to thank my adviser Dr. James Kubicki (Department of Geological Sciences-University of Texas El Paso) for guiding me every step of the way with my research, even after moving locations halfway through my graduate research.

1.0 INTRODUCTION

1.1 Research performed

The research performed in this study examines the use of alternative fluids, instead of water, in hydraulic fracturing. Research has shown that alternative fluids, such as gases or supercritical fluids, produce larger and more complex fractures, making it possible to extract a larger volume of hydrocarbons (*Alpern, 2013)*. Consequently, examining CO_2-shale interaction from a molecular approach may shed light on interfacial interactions that lead to a larger fracture, or a fracture with a greater radial extent. In this study, molecular modeling is used to compare water and supercritical CO_2 ($scCO_2$) interactions with illite (a common component of the Marcellus Shale and other shale gas formations) *(Brantley et. al., 2011)*. The interfacial energies of illite with $scCO_2$ and water (i.e., the energy of interaction between the two components) are derived from these simulations at a pressure and temperature relevant to shale gas extraction (e.g. T=60^{o}C and P=300 bar) *(Wright, 2014)*. A fluid with a smaller interfacial energy with the shale can be expected to yield a larger fracture network because it would more readily enter the shale and flow throughout the rock. As fluid is added and the pressure in the rock builds up, a greater fracture network would be produced. With a greater fracture network, a larger volume of hydrocarbons could then be extracted.

A radial distribution function (RDF) analysis was performed on each of the models to determine the distance between elements. An angular distribution function (ADF) analysis was performed to examine how illite surfaces affect the orientation of fluid molecules in the illite pores. A root-mean-squared displacement (RMSD) analysis determined how the illite surfaces affect the motion of the fluid molecules in the illite pores as they equilibrate. The RDF, ADF,

and RMSD analyses shed light on the specific chemical interactions that yield the corresponding interfacial energies between the fluids and illite.

1.2 Implications of research

The research presented in this study uses molecular modeling to examine $scCO_2$-clay interactions from a novel perspective. Researchers have primarily studied these interactions with regards to carbon sequestration (*Bao et al. 2013, Botan et al. 2010, Cygan et al. 2012, McCaughan et al. 2013, Myshakin et al. 2013, Schaef et al. 2013, Schaef et al. 2014*). By finding the interfacial energies between $scCO_2$-illite and examining the underlying molecular interactions that lead to these properties, the petroleum industry could have a solid scientific foundation giving them confidence as to which hydraulic fracturing fluid will work more effectively ($scCO_2$ or water).

1.3 Hypothesis

The interaction energy between illite and CO_2 should be smaller than the interfacial energy with water; the thermodynamic phase of CO_2 will cause the compound to interact less with the K^+ atoms at the surface of the illite grains. This lower interfacial tension with the surface is the factor that leads to a higher complexity of fractures with $scCO_2$, as seen in (*Alpern, 2013*) because the $scCO_2$ is better able to diffuse into nanopores and nucleate fractures in comparison to water.

2.0 BACKGROUND

2.1 Hydraulic fracturing fluids used today

Hydraulic fracturing is a process used to extract natural gas in shale rocks in previously unreachable locations. In this process, water and other additives are used to fracture open the rocks, creating interconnected fractures that allow fluid access by increasing permeability and and by providing access for gas in the shale to either flow or diffuse across fracture walls and then to flow to the well. Water is the most common primary fracturing fluid used today. As of 2012, 95 percent of all fracking in the United States was done with water (*Lockard, 2013*). This is because water is so readily available and industry knows how to use it effectively; therefore it is low-cost. However, in water-scarce regions, such as China, it could be too expensive to use water as a fracturing fluid. If another, more abundant fluid was used, fracking would be much more practical. There are also many citizens who have concerns about migration of the water with chemical additives out of the fractured rock; they believe that the water could migrate out of the rock into underground water supplies, or believe it is unethical to pump toxic chemicals into the ground. If a cleaner fluid was used, this could alleviate the fears of many. Finally, most importantly, water may not be the most effective fracturing fluid in general. Typically, the recovery factor for shale gas in fracking ranges from 15-25% with water as the fracking fluid (*Hester, 2013*). That means 75-85% of the gas is typically left behind in the formation.

Researchers and companies have been looking into using liquefied gas as a fracturing fluid because it should theoretically produce more complex fractures. More complex fractures yield a greater volume of hydrocarbons because with larger, more interconnected fractures, there are more pathways for hydrocarbons to flow out of the rock to the well (*Alpern, 2013*). One of the leaders today in utilizing unconventional fracturing fluids is the Canadian company named

GasFrac, which uses propane as a fracturing fluid. Eric Tudor, an official with GasFrac, claims that the company has drilled over 2,000 wells with propane fluid. He also claims that the propane fracks yield a better volume of hydrocarbons because "if you're using water, the water can actually block off or at least impede the flow of hydrocarbons" (*Galbraith, 2013).* This occurs because water is immiscible with the hydrocarbons. Glenn Gesoff, an official with BP, also states that his company is looking into using waterless fracking, with propane, CO_2, and nitrogen among the fracturing fluids being studied (*Galbraith, 2013)*. GE is also working on a $10-billion research program that is aimed at using captured CO_2 for fracking (*Maverick, 2014*).

2.2 Advantages of $scCO_2$ as a hydraulic fracturing fluid

$ScCO_2$ is one of the most interesting prospects for fracturing fluid. With growing concerns for anthropogenic climate change, many scientists and politicians are calling for the enforcement of reduced carbon emissions. As a society, we are unlikely to reduce our energy intake, and alternative energies are not yet built to capacity to replace fossil fuels. Carbon sequestration could be an effective method of reducing CO_2 emissions to the environment. In this process, CO_2 is first captured from a plant, compressed and transported, and then injected underground into deep rock formations. Experiments have proven than $scCO_2$ can be stored successfully in fractured shale gas formations (*Bacon et al. 2015, Busch et al. 2008, Heller and Zoback, 2014, Khosrokhavar et al., 2014*). If carbon taxes are imposed to further enforce greenhouse gas reduction, this process will likely be widely used. These developments are significant because if infrastructure is created to both capture and transport CO_2, $scCO_2$ becomes more economical as a fracking fluid. Another advantage of using $scCO_2$ as a fracturing fluid is that it could eradicate the problems of flowback water and could reduce the need for chemical additives (*Gensterblum et al. 2015*). The main hindrance today to using it as a fracturing fluid is

that it is expensive to capture and transport. If carbon sequestration becomes a necessity, this issue would be resolved because companies would be already incentivized to capture and transport CO_2.

In addition, $scCO_2$ may be a better fracturing fluid in areas where water is scarce. Although CO_2 is difficult to extract from the atmosphere, it may be the only option for areas that have limited water supplies. China is estimated to have the largest quantity of recoverable shale gas in the world, yet they also have a large shortage of water (*Hester, 2013)*. Northwest China has the largest area of recoverable shale gas, but is also one of the most arid regions of China (*Ma, 2012*). That is why using $scCO_2$ would be advantageous. Researchers such as Shen Zhonghou, a member of the Chinese Academy of Engineering, are working on technologies that use $scCO_2$ to extract shale gas. They have spent "nearly 4 million yuan and several years on research" (*Jing, 2012*). They have concluded in their research that $scCO_2$ is an effective fracturing fluid for drilling (*Jing, 2012*).

Because it is supercritical, $scCO_2$ create a lower stress with the rock. The fluid then should have minimal interfacial tension with the shale and should seep into nanopores at lower pressures. The fluid will then expand and would be adsorbed by the clay minerals, causing the fluid to stay in the formation. This would result in a larger pore network. The $scCO_2$ injection would also cause desorption of methane, resulting in greater recovery (*Bacon et al., 2015*).

2.3 Past experimental research with $scCO_2$ fluid

Alpern et al. (2013) completed experiments at Pennsylvania State University to test the effectiveness of different fracturing fluids in cracking polymethyl methacrylate (PMMA). (PMMA has been consistently used in laboratory experiments to model shale because PMMA has known physical properties, has the ability to carry large loads of stress comparable to rock,

and is transparent, so experimenters can observe fracture propagation). As seen in Figure 1a, it was found that the gases and $scCO_2$ consistently created fractures in the material with more complex fractures, thus making them more effective fracturing fluids (*Alpern, 2013*). The complexity index seen in Figures 1b-1f takes into account both the shape of the fracture, as well as the extent of the fracture. A higher complexity index was given to fractures with more complex shapes and of greater sizes. The experiments demonstrated that water yielded the least complex fractures, whereas other fluids, including $scCO_2$ yielded more complex fractures.

Ishida et al. (2012) conducted an experiment in which CO_2 was injected into cubic, isotropic granite blocks to create fractures. They found the breakdown pressures and fracture sizes and shapes formed from injecting various fluids: l-CO_2, sc-CO_2, water, and viscous oil fluids (*Ishida et al., 2012*). The fracture sizes and shapes were measured by finding the fractal dimensions (FD); higher fractal dimensions correspond to fracture dimensions that extend more three dimensionally rather than along a flat plane (*Ishida et al., 2012*). The breakdown pressures indicate the ease with which the fluids can be pumped into the granite; a lower breakdown pressure indicates that the fluid can fracture the rock more readily. The breakdown pressures and fractal dimensions for each of the fluids are shown in Table 1.

Fracturing Fluid	Breakdown Pressure (MPA)	Average Fractal Dimension
l-CO_2	10.56	1.63
sc-CO_2	8.44	2.42
Oil	17.9	N/A
water	16.5	N/A

Table 1: Breakdown Pressure and Fractal Dimensions for various Fracturing Fluids in Granite (Ishida et al., 2012)

Overall, $scCO_2$ had the lowest breakdown pressure, so fractured the granite more readily; lower amounts of $scCO_2$ would have to be pumped into the granite to cause fractures (*Ishida et al., 2012*). Although the fractal dimensions for oil and water were not found, it can be implied that $scCO_2$ would have the highest fractal dimensions, and thus create a larger fracture network (*Ishida et al., 2012*). In both Alpern's and Ishida's research, the blocks modeling shale were isotropic. In real life, shale is anisotropic because of pre-existing fractures. Therefore, the experiments would not perfectly represent real-world results and further investigation would have to be performed into how isotropy would affect the fracturing fluids.

Hydraulic fracturing with $scCO_2$ will become economically viable if carbon sequestration becomes widely implemented. Research can be done today, to further investigate its effectiveness as a fracturing fluid, as well as to better understand the interactions between molecules that cause low-pressure fractures.

Heller and Zoback (2014) completed experimental work that investigated $scCO_2$ injection into shale gas reservoirs: the Barnett, Eagle Ford, Marcellus, and Montney reservoirs. They also did the experiment with pure illite and kaolinite to represent shales. They found that $scCO_2$ injection causes increased methane desorption, and that $scCO_2$ sorption would occur in the clay formations (*Heller and Zoback, 2014*). Heller and Zoback (2014) proved that the affinity that $scCO_2$ has for the clay formation would both cause methane to be removed from the formation and cause the $scCO_2$ to remain in the formation. Other similar experimental research found the same results. (*Bacon et al., 2015, Khosrokhavar et al., 2014*).

2.4 Past molecular modeling research looking at similar interactions

Our research uses density functional theory (DFT) molecular simulations to model the molecular interactions between the sc-CO_2 and shale that would lead to more complex fractures.

Past research has also used molecular simulations to look at these interactions, but mostly with regard to carbon sequestration. (*Bao et al. 2013, Botan et al. 2010, Cygan et al. 2012, McCaughan et al. 2013, Myshakin et al. 2013, Schaef et al. 2013, Schaef et al. 2014*). McCaughan et al. (2013), in particular, conducted similar research to our study. They used molecular dynamics (MD) simulations to model the interfacial properties between sc-CO_2 and quartz, to determine how much CO_2 could be stored in shale formations. They specifically examined the contact angles between water and quartz and CO_2 and quartz. (*McCaughan et al., 2013*). Schaef et al. (2014) also performed similar research regarding carbon sequestration in kaolinite surfaces. They specifically examined the adsorption energy of CO_2 on kaolinite (*Schaef et al.* 2014). There is no published research, to the author's knowledge, that examines interactions of scCO_2 in molecular simulations that bear on hydraulic fracturing.

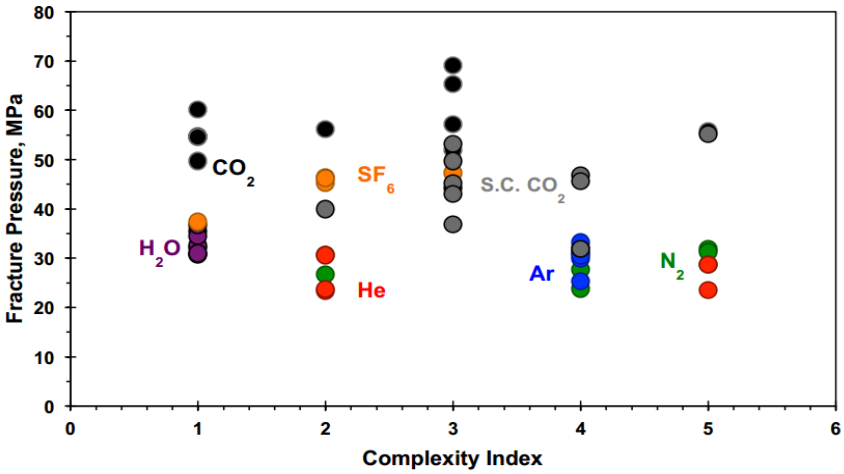

Figure 1a: Experimental results with various fracturing fluids in PMMA; PMMA is used in PSU lab to "model" shale (Alpern, 2013)

Figure 1b: Experimental results of Fracture with Complexity Index of 1; 1 is the least complex type of fracture (Alpern, 2013)

Figure 1c: Fracture with Complexity Index of 2 (Alpern, 2013)

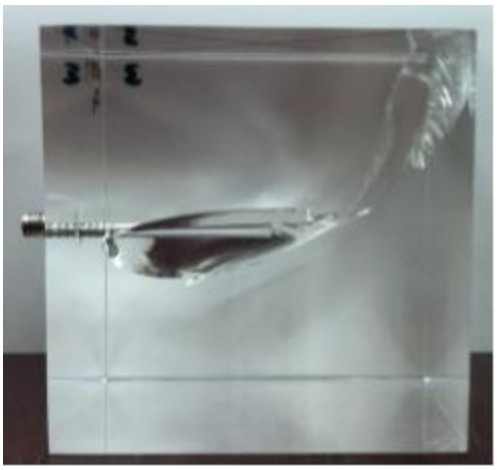

Figure 1d: Fracture with Complexity Index of 3 (Alpern, 2013)

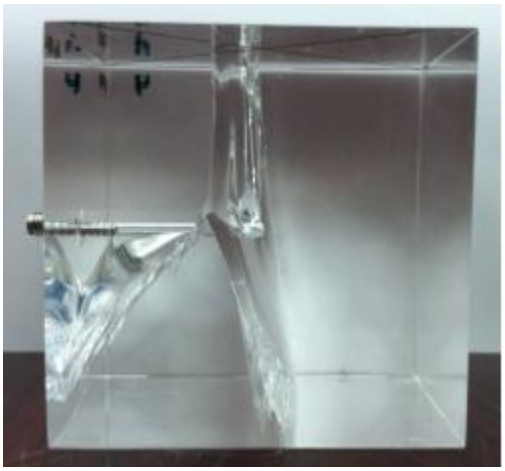

Figure 1e: Fracture with Complexity Index of 4 (Alpern, 2013)

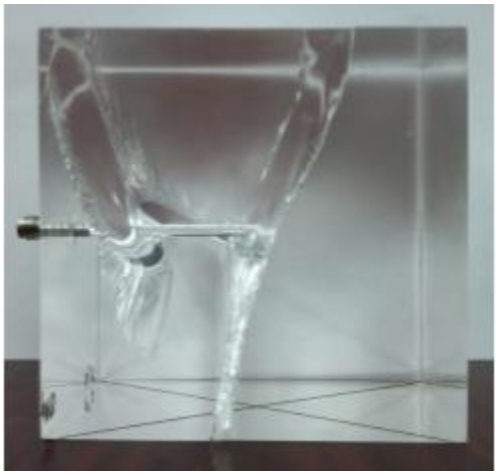

Figure 1f: Fracture with Complexity Index of 5; 5 is the most complex type of fracture (Alpern, 2013)

3.0 COMPUTATIONAL METHOD

3.1 Theoretical research vs. experimental research

Molecular simulations model the behavior of the interaction of compounds. Molecular simulations, such as molecular dynamics (MD), have become popular for predicting fluid properties in geological conditions (*Cygan, 2001*). Experimental methods can also study this behavior, and will provide more accurate and realistic data, but such experiments do not provide atomistic details in many cases (*Cygan, 2001*). In addition, experiments are commonly limited in temperature and pressure range. Skepticism regarding the usefulness of molecular simulation exists because they are virtual results, but they can be useful complements to experimental methods because they are independent of experimental data (i.e., they are not fitted results), and simulations are not limited by constraints on temperature and pressure (*Bao et. al, 2013*). Theoretical methods are meant to complement experiments by aiding interpretation of the information observed (*Cygan, 2001*). Also, once results for molecular modeling are found to be accurate, by comparing with experimental data, the result is a better understanding of what molecular properties lead to observed phenomena.

3.2 Molecular modeling methods

Molecular modeling investigates phenomena at an atomic scale: in the range of femtoseconds to nanoseconds in time, and Ångstroms to nanonmeters in distance (*Cygan, 2001)*. The research in this study specifically used computational quantum methods. Molecular modeling aims to measure interatomic interactions to find the total energy of a molecular system (*Sherman, 2016).* Quantum mechanical molecular modeling methods specifically use quantum calculations to evaluate interatomic interactions, with minimal input from empirical parameters (*Cygan, 2001*). Density functional theory (DFT) is the specific quantum mechanical method used

in our research. DFT uses the density of electrons and the interaction between the different electron densities in a system to yield an energy (*Cygan, 2001*). Jones and Gunnarsson (1989) review DFT methods; the following articles also further examine DFT theory: Payne et al. (1992) and Milman et al. (2000).

One of the hindrances of quantum mechanical methods, such as DFT, is that the results have no relationship to macroscopic thermodynamic properties (*Sherman, 2016*). The energies yielded from a DFT simulation have no relationship to anything measurable on the real-world scale. Macroscopic properties, such as N (moles), V (volume), T (temperature), P (pressure), or E (potential energy) are associated with a large number of microstates (*Sherman, 2016*). By sampling a large number of these microstates, the macrostate can be derived. This is the method employed in molecular dynamics (MD) simulations. In our research specifically, N (moles), V (volume), and T (temperature) are constrained, and over a period of time, the macrostate energy is derived. This energy is useful on the real-world scale; therefore, the results can be compared to experimental data.

Our method of modeling combines both quantum (DFT) and classical molecular mechanics methods (MD) and is appropriately called a DFT-MD simulation. In order to yield potential energies, forcefields are employed. Forcefields describe "the energy of interaction for an assemblage of atoms" (*Cygan, 2001*). The DFT simulations provide input parameters for the forcefields, and the MD simulations sample a large number of microstates, yielding a final macroscopic energy.

3.3 Molecular modeling used in this study

There are two sets of simulations that concern this research, energy minimizations (or geometry optimizations) and molecular dynamics simulations. (Both of these simulations

incorporate DFT as force field inputs). An energy minimization is a molecular mechanic simulation that obtains a stable configuration for a compound or group of atoms. A major difference between the energy minimized structure and molecular dynamics simulations is that the temperature is at 0 K in the former. Figure 2 shows the results of an energy minimization for an assemblage of 63 H_2O molecules. The model structure of this minimum can be compared to the experimental structure of water.

A molecular dynamics simulation obtains an average energy where certain properties are input, such as temperature, volume, and composition (i.e., and N-V-T ensemble). Figures 3 and 4 show an example of a MD run for an assemblage of illite and 63 H_2O molecules. The temperature was set to 333K, and the model system converged to this value after approximately 50,000 steps of 0.5 fs. An average energy configuration of -2367.2 eV was obtained at that temperature (Fig. 4). A molecular modeler will often run energy minimizations and molecular dynamics interchangeably. For instance, we ran an energy minimization for a model system first, to obtain a stable structure. We then ran MD simulations to set it at certain temperature. We may then run another energy minimzation to find the stable structure and energy.

3.4 Programs used

The Vienna Ab-initio Simulation Package (*VASP, 2015*) was the program used to run energy minimizations and MD simulations for our phases of interest: illite, water, and $scCO_2$. VASP is a plane-wave code for ab-initio DFT calculations and runs on Linux.

Materials Studio (*Accelrys Inc., San Diego, CA*) is another program used in our research. This program was used to build and visualize the models. The configurations from this program are then transferred into VASP. These configurations were used as initial structures in energy minimizations and MD simulations. We used Materials Studio to run classical force field

simulations to obtain starting configurations to input to VASP. Once the simulations were run in VASP, the structures were transferred to Materials Studio to be viewed. The conversions between Materials Studio *.car file formats and VASP formats were done using a perl script written by Andrei V. Bandura (St. Petersburg State University, Russia).

3.5 Model stuctures

One goal of our research was to calculate the interfacial tensions, or interaction energies, between illite+scCO_2 and illite+water. Illite was chosen because it is the most abundant phase in the Marcellus Shale (*Hosterman et al., 1983*). Two different models for illite were used, one with no K^+ atoms ($Al_{16}Si_{32}O_{96}H_{16}$) and the other with 8 K^+ atoms ($K_8Al_{24}Si_{24}O_{96}H_{16}$) shown in Figures 5-8. In previous research, a number of illite models were found to be useful with a range of number of K^+ and a net zero charge. Our illite models were built to reflect that range. The illite model was provided by R.T. Cygan (Sandia National Laboratory). The illite surfaces reflected two illite surfaces with corresponding pore space to be filled with fluids. The size of the illite structures were 10.40 Å x 8.98 Å x 38.38 Å with about half of the structure occupied by pore space. The two illite molecules represented in Figures 5 and 6 have 14 H_2O molecules on the surface of the pore space, simulating wet pores. The two illite models represented in Figures 7 and 8 have 4 polymethyl methacrylate (PMMA) molecules on the surface of the pore space, simulating hydrocarbon saturated pores. PMMA is a molecule that has been used in past molecular simulations to model hydrocarbons, and is a simple hydrophobic surface, mimicking the behavior of hydrocarbons.

The number of molecules of H_2O and CO_2 in the pore space were chosen based on the pressure and temperature expected at the depths underground usually expected during hydraulic fracturing. With the pressure and temperature, equations of state help us find the density of each

of the compounds. We decided we would be working 5280 ft (1609 m) underground where temperature is expected to be at a range of 60-80^{o}C. The expected fluid phase pressure within the pores would be at a range of 300-600 bar based on a geothermal gradient of 0.03bar/ft underground (*Wright, 2014*). CO_2 and water were constrained at T=60^{o}C and P=300 bar. The temperature and pressure were converted to a density using the thermodynamic properties of CO_2 and water (*Peace Software).* The temperature and pressure for both of the fluids were chosen to be 60^{o}C and 600 bar, corresponding to a density of 0.970 g/cm^3 of scCO_2 in pore space and 1.007 g/cm^3 of water in pore space. These densities corresponded to a certain number of fluid molecules in pore space based on the volume of illite pore space as shown in Table 2. Molecular structures were then built with fluids in the pore space of illite. These structures are shown in Figures 9-12. For the structures: H=white, O=red, K=purple, Al=pink, Si=yellow, and C=black.

3.6 Parameters used for molecular simulations

After the initial structures were built in Materials Studio, energy minimizations were run in Materials Studio with the Universal force field (*Rappé et al., 1992*). They were performed with a convergence tolerance set an an energy of 1.0 x 10^{-4}kcal/mol, a force of 0.005 kcal/mol/Å and a displacement of 5.0x10^{-5} Å with the displacement setting corresponding to "Fine" quality. These strucutres were then transferred into VASP using the perl script 'car2poscar.pl' created by Andrei V. Bandura from St. Petersburg State University, Russia.

Each of the models were then energy minimized in VASP. In these runs, a "a conjugate-gradient algorithm is used to relax the ions into their instantaneous groundstate" (*VASP, 2015*). These models then underwent MD simulations, with the temperature parameterized to 333.33K. Standard PBE projector-augmented wave method potentials (*Blochl, 1994*) (*Kresse and Joubert,*

1999) were used. These potentials have been previously tested using standard DFT runs and have proved reliable and accurate up to an energy cutoff of 250eV (*VASP, 2015*). The Monkhorst-Pack scheme was used to generate a single k-point at the G point of the Brillouin zone. The energy cut-off was set to 400 eV for the plane wave basis set in the MD simulations. A higher energy cut-off value results in more accurate, but slower reults (*VASP, 2015*). The models were run at a "Medium" precision, which is sufficiently accurate; errors are less than 1 meV/atom (*VASP, 2015*). With this precision setting, the FFT gredits are reduced and ¾ of the required values are used (*VASP, 2015*). EDIFF was set to 10^{-4}, giving the total energy results siginificant to 4 figures. NSW was set to equal 5000 steps so there were a maximum of 5000 steps before each simulation run ended. ISPIN was set to equal 1, so non-spin polarized calculations are performed instead of spin polarized calculations (*VASP, 2015*). POTIM was set to equal 0.5, so there were 0.5 femtosecond time steps. THE DFT-D3 method was used to approximate the vddW energy (*Grimme et al., 2010*). The Verlet algorithm was also used to integrate Newton's equations of motion (*Verlet, 1967*). The forces are first calculated for the initial configuration. The second step is a predictor step and then the third step is a corrector step. If the line minimization is sufficiently accurate in this step, the next trial step is performed. This process repeats until reaching the desired number of steps. Each of the models were run for approximately 50,000 steps (25 ps) with each taking months to run. The models composed only of the fluid molecules were run with 4 processors, the illite models were run with 8 processors, and the illite models with fluids in pore space were run with 16 processors. The processors used were conducted with Advanced CyberInfrastructure computational resources provided by The Institute for CyberScience at The Pennsylvania State University (http://ics.psu.edu). The computations were run on two different architectures: Mellanox FDR infiniband for CPU

processing and the other uses Qlogic DDR infiniband (*LionX Systems*). After each of the MD simulations were run, energy minimizations were run in VASP to find final energies for each model.

3.7 Result derivations

DFT-MD would then be run for each of the structures followed by an energy minimization, resulting in an energy value for each structure.

From these energies, we can then find the following interfacial energies using the following equation:

$$Interfacial\ energy\ between\ illite\ and\ fluid = energy\ of\ illite\ with\ x\ number\ of\ molecules\ of\ fluid\ in\ pore\ space - x\ of\ molecules\ of\ fluid - energy\ of\ illite$$

2 different configurations of illite, 2 different fluid monolayers, and 2 different types of hydrofracturing fluids would yield 8 different interfacial energies:

Interfacial energy between illite-8K^+ with H_2O monolayer and CO_2

Interfacial energy between illite-0K^+ with H_2O monolayer and CO_2

Interfacial energy between illite-8K^+ with H_2O monolayer and H_2O

Interfacial energy between illite-0K^+ with H_2O monolayer and H_2O

Interfacial energy between illite-8K^+ with PMMA monolayer and CO_2

Interfacial energy between illite-0K^+ with PMMA monolayer and CO_2

Interfacial energy between illite-8K^+ with PMMA monolayer and H_2O

Interfacial energy between illite-0K^+ with PMMA monolayer and CO_2

3.8 Additional results to derive

In addition to interfacial energies, analysis was done to find the underlying molecular interactions that led to the interfacial tensions. Radial distribution function (RDF) analysis, angular distribution function (ADF) analysis, and root-mean-squared displacement analysis

(RMSD) were performed with codes written in C++ provided by Mark DelloStritto (The Pennsylvania State University).

RDF analysis measures the distance between elements in each of the models. This analysis determines if illite structures affect the distance between the molecules of fluid. The distances are driven by the various forces of interaction: H-bonding, ion-dipole and van der Waals forces for H_2O and van der Waals forces for CO_2. If the distances between molecules of fluid are the same for the fluid models alone and the fluid molecules in the pore space of illite, then the illite has minimal effect on the fluid molecules. From the RDF analysis, a graph can be constructed showing RDF vs distance in (Å). Peaks that appear on the graph correspond to the characteristic distance of certain force. For instance for H_2O molecules, there will be a peak at around 2 Å.

ADF analysis determines the orientation of each of the fluid molecules. This analysis is performed to probe how illite structures affect the orientation of the fluid molecules in pore space. From the ADF analysis, a graph can be constructed showing ADF vs angle. The angle is found from a vector from the central atom (C in CO_2 and O in H_2O) to the valence atom (O in CO_2 and H in H_2O). There are two vectors for each fluid molecule. The angle (Φ) is then the angle between each of these vectors and the z-axis. The z-axis is a vector pointing directly away from the illite structure. A cartoon depiction of angles for a sample CO_2 molecule in illite is shown in Figure 13. From the graph of ADF vs angle, a normal bell curve centered at 90^o would depict a completely random orientation of molecules. This is because there are more possible configurations of angles closer to 90^o than at 0^o or 180^o. This concept is further articulated in Figure 14. If the fluid orientation results are different between the fluids by themselves and the fluids in pores of illite, than the illite is affecting the orientation of fluids.

RMSD analysis was employed to examine the diffusion of the fluids in the pore space. In this analysis, the movement of each of the fluid molecules were monitored in the x and y directions, or the directions parallel to the illite surface. This movement over time yields an average diffusion coefficent for each fluid in each model. The diffusion coefficients can be compared to determine how the illite surfaces affect the diffusion of fluids in the pore space. These coefficients can also be compared to relevant experimental data.

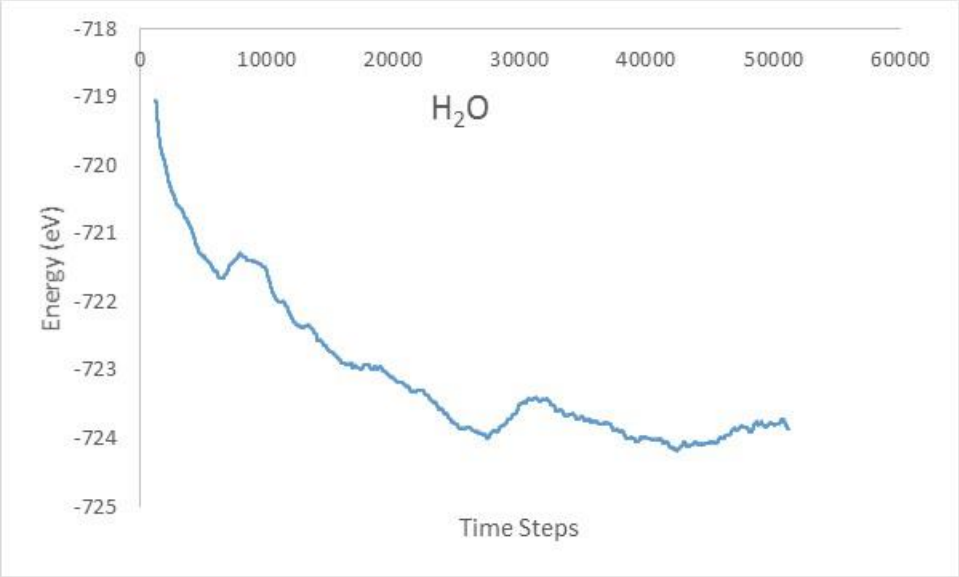

Figure 2: Energy minimization simulation for 63 molecules of H_2O ran for about 50,000 time steps; stabilized at -723.5eV

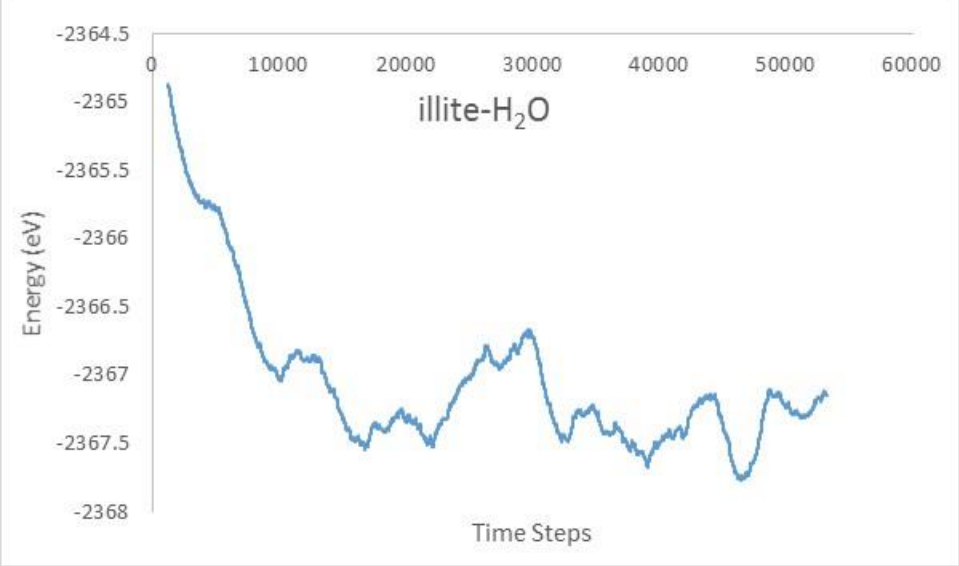

Figure 3: Molecular dynamics for 63 molecules of H_2O in pores of illite ran for about 50,000 time steps; temperature was parameterized at 333.33K and the energy stabilized at -2367.2eV

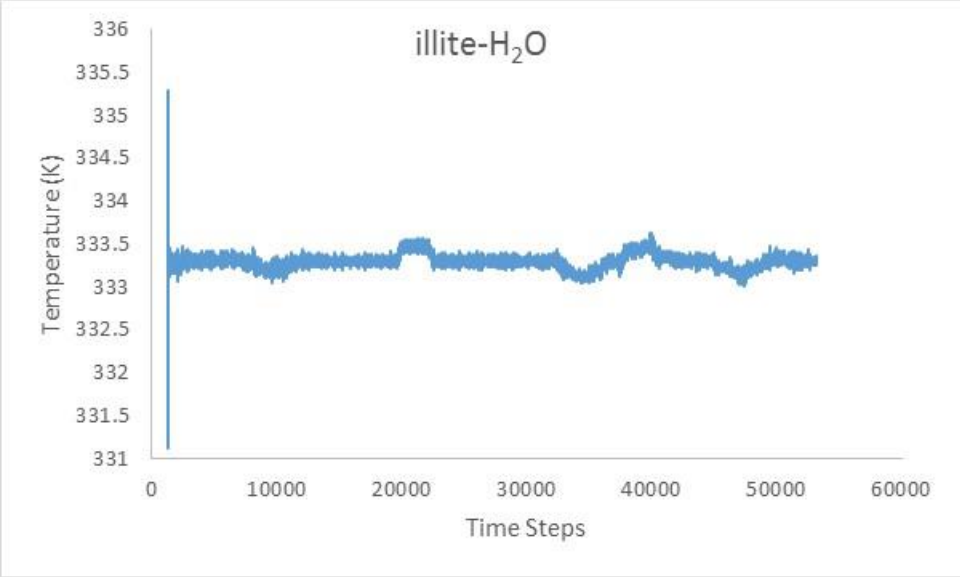

Figure 4: Molecular dynamics for 63 molecules of H_2O in pores of illite ran for about 50,000 time steps; temperature was parameterized at 333.33K

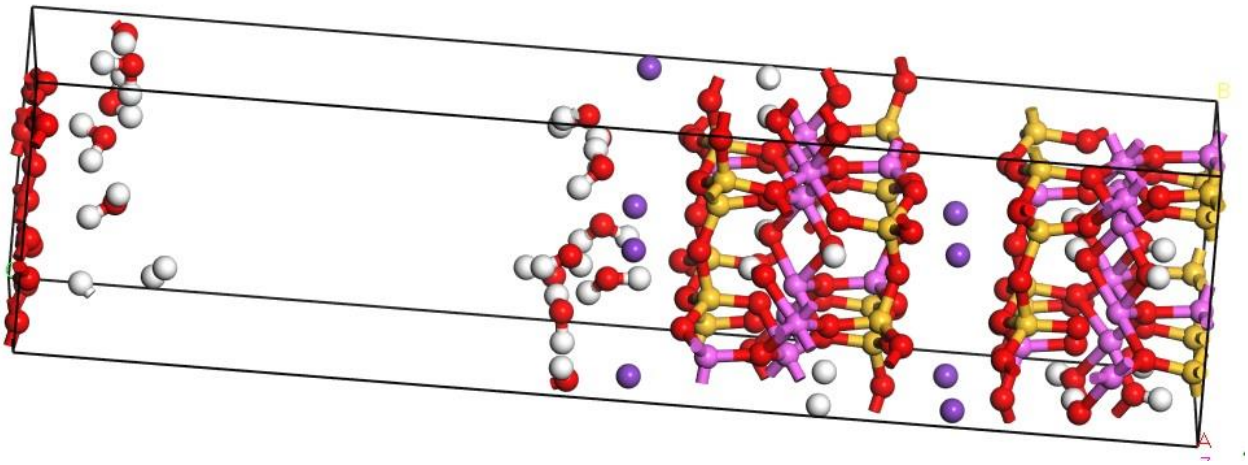

Figure 5: Materials Studio model portraying $K_8Si_{24}Al_{24}O_{80}(OH)_{16}$ with 14 H_2O molecules (illite-8K^+-water)

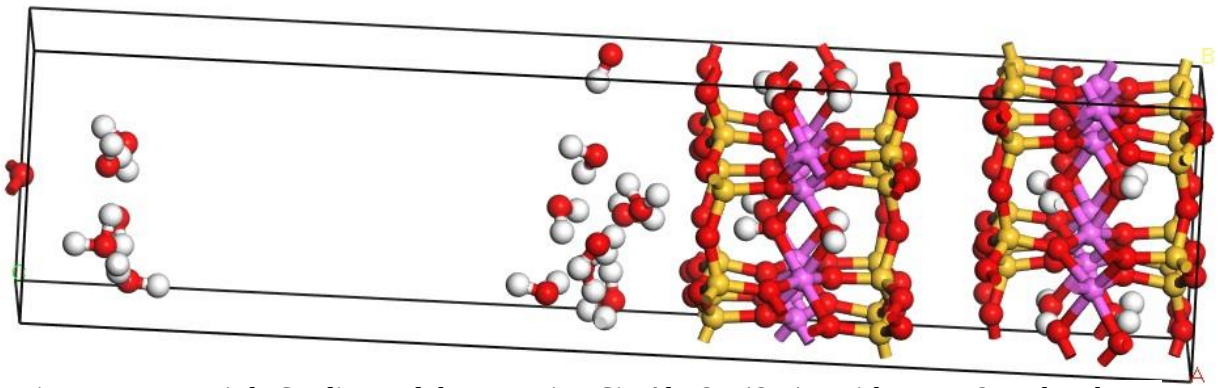

Figure 6: Materials Studio model portraying $Si_{32}Al_{16}O_{80}(OH)_{16}$ with 14 H_2O molecules (illite-0K^+-water)

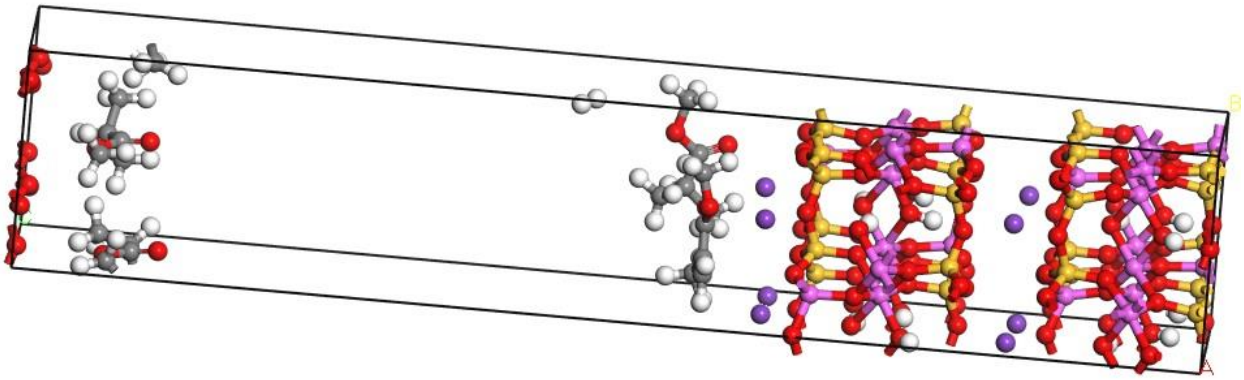

Figure 7: Materials Studio model portraying $K_8Si_{24}Al_{24}O_{80}(OH)_{16}$ with 4 PMMA molecules (illite-8K^+-PMMA)

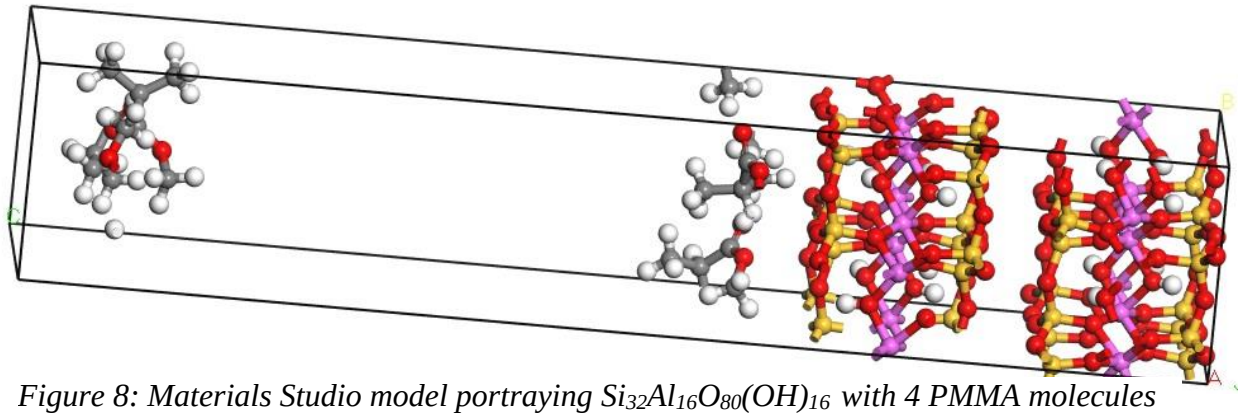

Figure 8: Materials Studio model portraying $Si_{32}Al_{16}O_{80}(OH)_{16}$ with 4 PMMA molecules (illite-0K^+-PMMA)

Illite model	Number of CO_2 molecules in pore space	Number of H_2O molecules in pore space
$K_8Si_{24}Al_{24}O_{80}(OH)_{16}$ ($8K^+$ model)	25	49
$Si_{32}Al_{16}O_{80}(OH)_{16}$ ($0K^+$ model)	28	54

Table 2: number of fluid molecules in pore space for each illite model

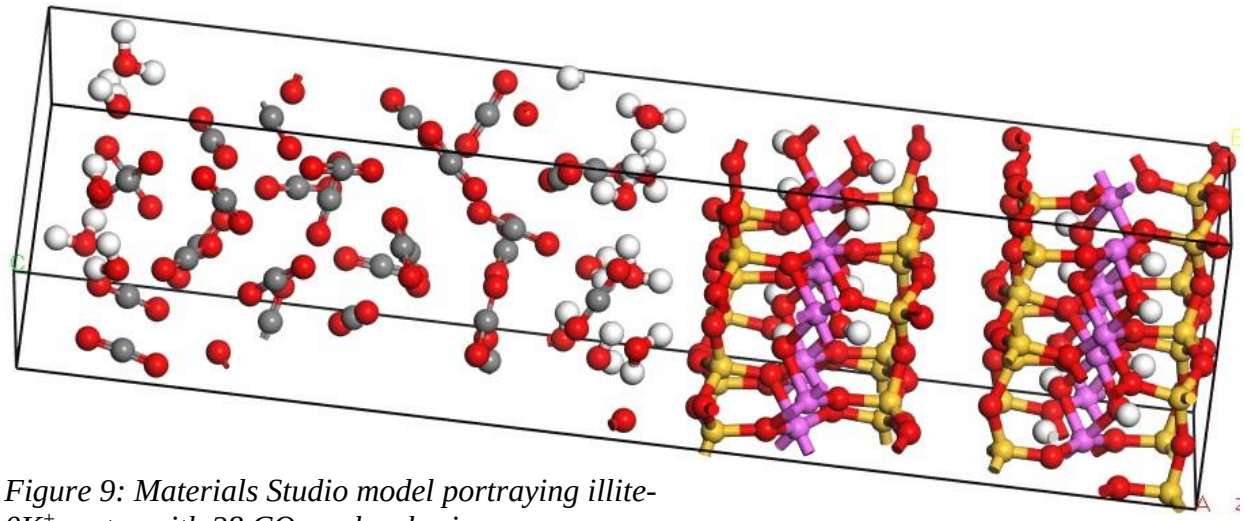

Figure 9: Materials Studio model portraying illite-0K^+-water with 28 CO_2 molecules in pore space

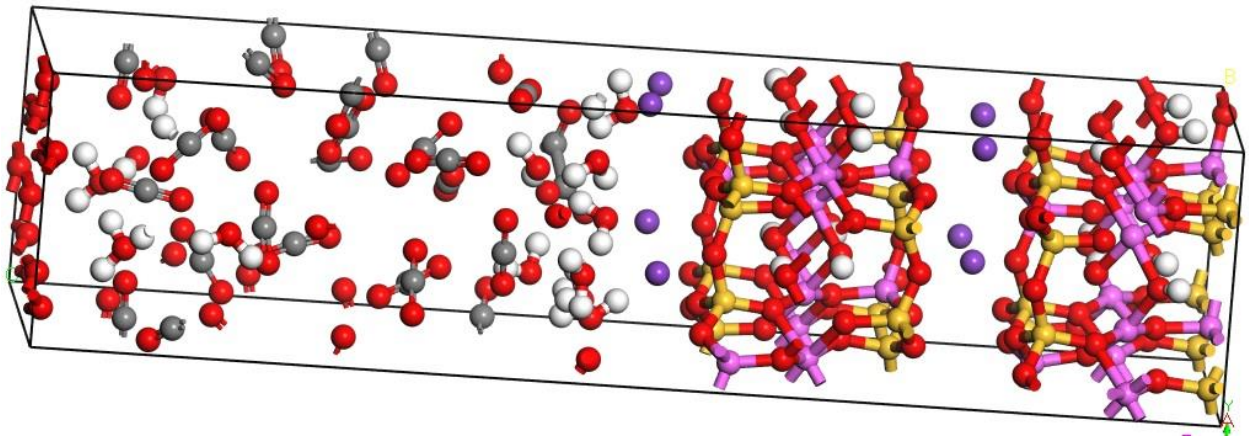

Figure 10: Materials Studio model portraying illite-8K^+-water with 25 CO_2 molecules in pore space

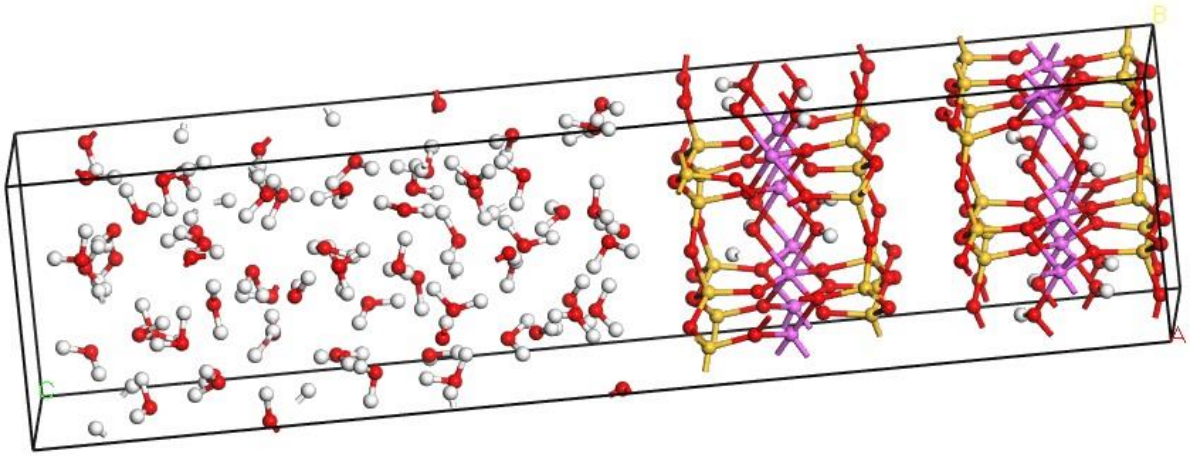

Figure 11: Materials Studio model portraying illite-0K^+-water with 54 H_2O molecules in pore space

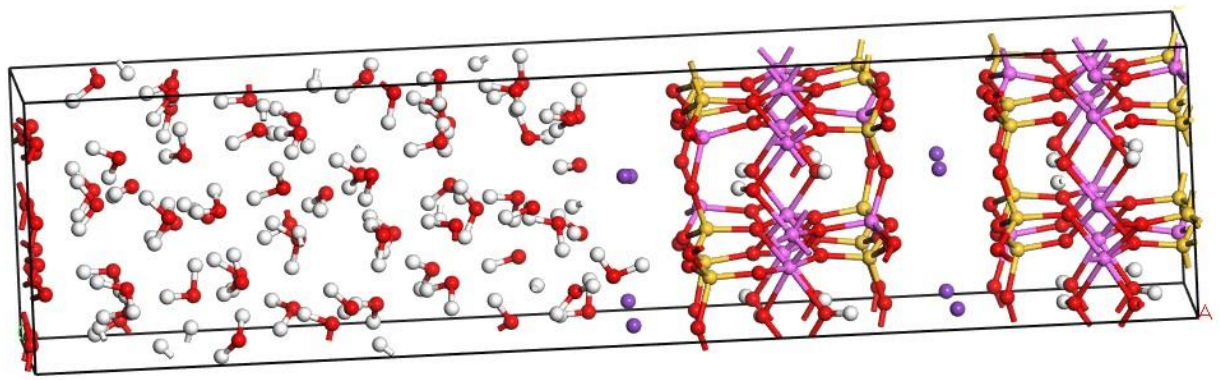

Figure 12: Materials Studio model portraying illite-8K^+-water with 49 H_2O molecules in pore space

Figure 9-12 illite with PMMA monolayer and fluids

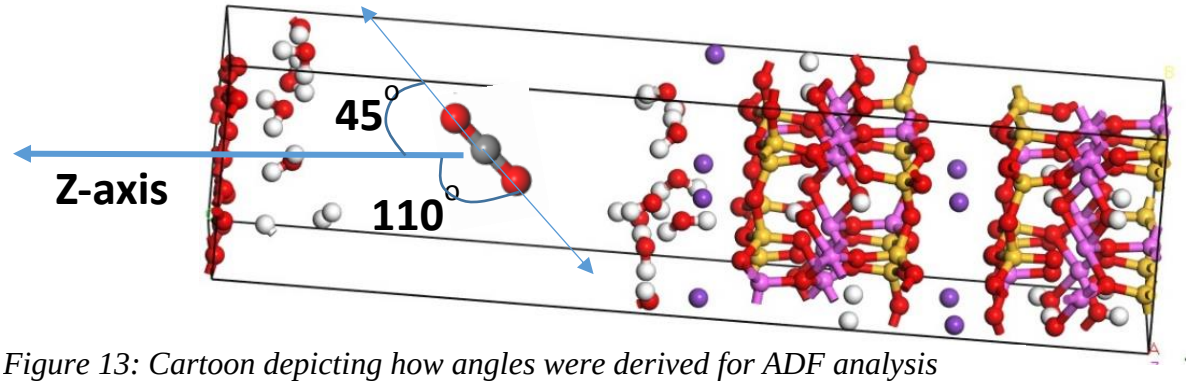

Figure 13: Cartoon depicting how angles were derived for ADF analysis

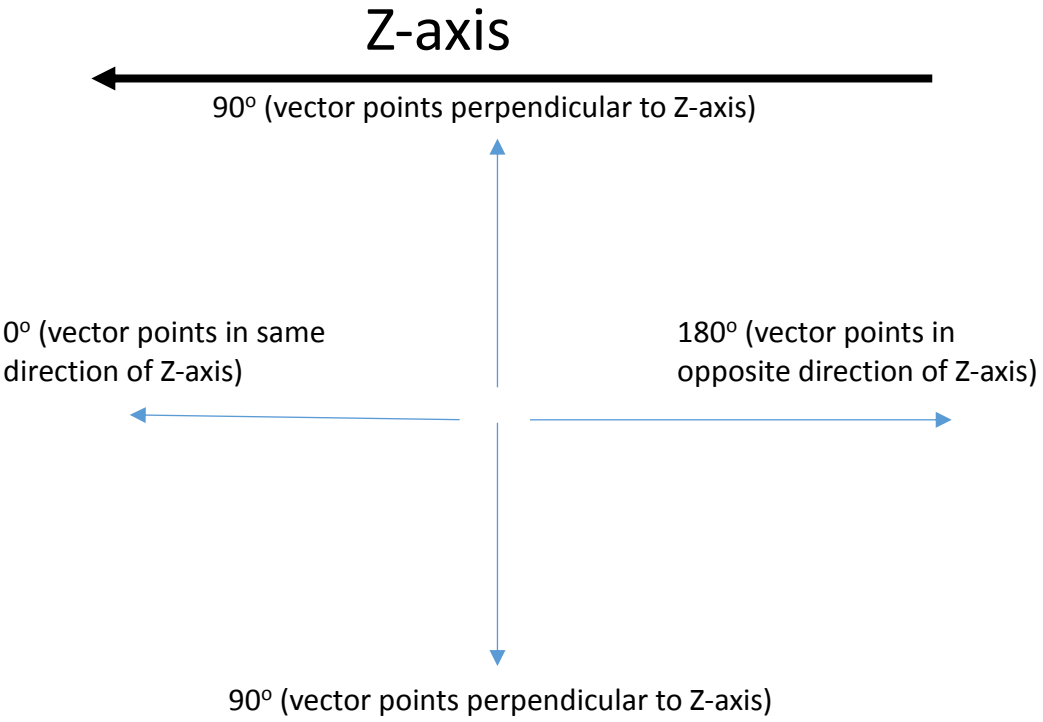

Figure 14: How angles were derived for ADF analysis

4.0 RESULTS AND DISCUSSION

4.1 Interfacial tension

The interfacial tensions were derived between $scCO_2$ and illite and water and illite with the two different illite models ($0K^+$ and $8K^+$) and the water monolayer and PMMA monolayer. The results for the interfacial tensions are shown in Table 3.

Surface	Monolayer	Fluid	Interfacial Tension (J/m^2)
Illite with no K^+	Water	$scCO_2$	0.01261
Illite with 8 K^+	Water	$scCO_2$	0.02198
Illite with no K^+	Water	Water	0.01112
Illite with 8 K^+	Water	Water	0.04220
Illite with no K^+	PMMA	$scCO_2$	0.00660
Illite with 8 K^+	PMMA	$scCO_2$	0.01344
Illite with no K^+	PMMA	Water	0.00285
Illite with 8K+	PMMA	Water	0.00088

Table 3: Interfacial tensions from energy-minimized structures

For the rest of the paper the following abbreviations will be used for each of the illite structures:

Surface: Illite with No K^+ Monolayer: Water Abbreviation: Illite-$0K^+$-water

Surface: Illite with 8 K^+ Monolayer: Water Abbreviation: Illite-$8K^+$-water

Surface: Illite with No K^+ Monolayer: PMMA Abbreviation: Illite-$0K^+$-PMMA

Surface: Illite with 8 K^+ Monolayer: PMMA Abbreviation: Illite-$8K^+$-PMMA

Illite-$0K^+$-water has a similar interfacial tension with $scCO_2$ fluid and water fluid (0.01261 J/m^2 vs 0.01112 J/m^2). Illite-$8K^+$-water has a much higher interfacial tension with water than with $scCO_2$ (0.04220 J/m^2 vs 0.02198 J/m^2). The Illite-$8K^+$-water models have higher interfacial tensions with both fluids compared to the Illite-$0K^+$-water models (0.02198 J/m^2 and

0.04220 J/m^2 vs 0.01261 and 0.01112 J/m^2). The fluids all form a significantly lower interfacial tension with the Illite-PMMA models with the exception of sc-CO_2 with illite-8K^+-PMMA (0.01344 J/m^2).

4.2 Comparison of interfacial tensions with experimental results

The accuracy of our results were tested by comparing them with relevant experimental data. Molecular modeling studies attempt to represent atomic interactions and cannot account for every factor that would affect the results. With relevant experimental data, however, it can be verified if other factors affect the molecular modeling results. Experimental studies have been performed to determine the interfacial tension between scCO_2 and a surface in the context of CO_2 sequestration. The surfaces used for these experiments were quartz and PTFE; they were assumed to behave similarly to illite. This assumption is more generally true for the illite-0K^+ models because quartz and PTFE are also neutral, hydrophobic surfaces. In the experiment, the interfacial tension between CO_2 and water was calculated, with water existing as oil-wet quartz (*Espinoza et al., 2010*). The water droplets on the surface behave similar to the water monolayers on the illite model. The interfacial tension, in this experiment, between CO_2 and the solid surfaces were computed at various pressures and at a temperature of 298 K (*Espinoza et al., 2010*). CO_2 is very close to a supercritical state at a pressure of 10 MPa (100 bar), one of the pressures used in the experiment. Another experimental study observed the interfacial tension between water and a solid surface, PTFE (*Dickson et al., 2006*). The interfacial tensions were measured between water and PTFE at a range of pressures, from 0.1-7 MPA (10 to 70 bar) (*Dickson et al., 2006*). Table 4 shows a summary of the interfacial tensions from the two experimental studies and this study.

Surface	Fluid	Source	Interfacial Tension (J/m^2)
Illite-0K^+-water	$scCO_2$	This study	0.01261
Illite-0K^+-PMMA	$scCO_2$	This study	0.00660
Illite-8K^+-water	$scCO_2$	This study	0.02198
Illite-8K^+-PMMA	$scCO_2$	This study	0.01344
PTFE with water droplets	l-CO_2	Espinoza et. al	0.02-0.03
Oil-wet quartz with water droplets	l-CO_2	Espinoza et. al	0.02-0.03
Illite-0K^+-water	Water	This study	0.01112
Illite-0K^+-PMMA	Water	This study	0.00285
Illite-8K^+-water	Water	This study	0.04220
Illite-8K^+-PMMA	Water	This study	0.00088
PTFE	Water	Dickson et. al	0.025

Table 4: Comparison of fluid-substrate interfacial tensions between experimental research and theoretical research from this study

Table 4 shows that the interfacial tensions from the experimental studies are in the same order of magnitude as the interfacial tensions from this study. This suggests that the results from this study are reasonably accurate. The absolute order of magnitude of interfacial tensions, however, are not as important as the relative order of magnitudes between the two fluids and illite. The relative magnitudes of the interfacial tensions between $scCO_2$/illite and water/illite determine their comparative effectiveness as hydraulic fracturing fluids.

4.3 Radial distribution function analysis

The final MD-structures underwent RDF, ADF, and RMSD analysis. The results for the RDF analysis for models with H_2O fluid are shown in Figure 15. The 49 H_2O fluid model and 54 H_2O model show the structure of H_2O under normal conditions. There is a peak at 1.7 Å, depicting strong hydrogen bonding; there is also peak at 3.2 Å, depicting O-O bonds. Most of the H_2O fluids in the illite pores have similar structures, indicating that the illite is not greatly

affecting the distance between the molecules of fluids. The model with H_2O in the illite-$8K^+$-water pore space has a slightly earlier H-bonding peak, around 1.6 Å. This peak is shifted likely because of the hydrophobic nature of the siloxane surface; the H_2O molecules are more strongly attracted to one other because they cannot form favorable interactions with the surface. The model with H_2O in the illite-$8K^+$-water pore space has a small peak at 2.2 Å; this peak doesn't occur in the other models. This peak is indicative of weak H-bonding. The weaker H-bonding is caused by siloxane linkages at the surface of the illite which are not hydrophilic.

Del Ben et al. (2015) performed similar RDF calculations with H_2O molecules to analyze MD simulations. The H_2O molecules had a similar density to the density in this study, ≈1 g/cm^3. Their simulations were parameterized at T=295K and P=1 bar. The pressures are much smaller than the pressures in our study and the temperatures are also significantly smaller. Our simulations were run at T=333K and P=600 bar. A comparison of the RDF results between our study and the Del Ben et al. (2015) study are shown in Table 5. The values shown for Del Ben et al. (2015) are averaged for the different H_2O models in the sumaltion. The H_2O molecules in their study have rigid bonds; in our study the bonds can shorten and elongate. Their results show O-O RDF peaks at 2.8 Å which are significantly lower than the O-O RDF peaks in this study, around 3.2 Å. This discrepancy is likely due to the lower temperature and pressure used in their study.

Soper (2013) also performed RDF calculations for H_2O using radiation total scattering experiments. The RDF results for H_2O were measured at T=300K. Figure 16 shows the RDF results from that study. Table 5 also includes the Soper (2013) results. The results are similar to our results, although the RDF peaks in our study have a narrower O-H peak with a shorter maximum and the O-O peak is displaced to longer distances, in the order of a few tenths of an

Ångstrom. These errors are acceptable due to the inaccuracies in DFT reproduction of H-bonds and the differences in P and T between our simulation and the experiment in Soper (2013).

Model	Source	1st peak	H-bonding	2nd peak	O-O bond
		r (Å) O-H	RDF	r(Å) O-O	RDF
49 H_2O	this study	1.7	1.82	3.2	1.70
54 H_2O	this study	1.7	1.76	3.2	1.68
49 H_2O in illite-8K^+-water in pore space	this study	1.7	3.03	3.15	3.28
54 H_2O in illite-0K^+-water in pore space	this study	1.55	2.92	3.25	2.29
49 H_2O in illite-8K^+-PMMA in pore space	this study	1.7	5.56	3.2	4.81
54 H_2O in illite-0K^+-PMMA in pore space	this study	1.7	5.01	3.2	4.63
H_2O	Del Ben et al	N/A	N/A	2.78	1
H_2O	Soper	1.86	1.04	2.79	2.50

Table 5: Comparison of H_2O fluid RDF results from various studies

Figure 17 shows the RDF results for the models with CO_2 fluids. The graph begins at 1.2 Å and cuts off the large, constant C=O bond peak. The 25 CO_2 fluid model and the 28 CO_2 model show the structure of CO_2 under normal conditions, there are no molecules affecting the fluids.There is only one peak for the CO_2 molecules in illite-8K^+-water pore space at 2.4 Å. This peak corresponds to an oxalate molecule that forms near the edge of the illite pores. (*The oxalate molecule will be discussed later in the paper*). The CO_2 molecules do not create significant structural order so there are no other peaks. The lack of structure is due to the weakness of Van der Waals forces at the temperature of the simulations.

4.4 Angular distribution function analysis

ADF analysis was performed to determine the orientation of each of the fluid molecules. Figure 18 shows the ADF results for all of the models with H_2O fluids, averaged for ≈5

picoseconds. The 49 H_2O and 54 H_2O models form a bell curve centered close to 90°. This indicates that the dipoles of these molecules orient relative to the z-axis in a randomized manner, which is expected for a bulk fluid. The H_2O fluids in illite-0K^+-water pore space and in illite-0K^+-PMMA pore space also behave similarly. These results indicate that the illite-0K^+-water and illite-0K^+-PMMA surfaces do not affect the orientation of the H_2O molecules; the H-bonding between H_2O molecules is stronger than any interaction between the H_2O fluids and the illite-0K^+ surfaces. This result is expected given the hydrophobicity of the siloxane surface. The hydrophobicity is because of the lack of K^+, so the surface of the illite is not charged, and therefore does not influence the dipoles formed in the H-bonds between the H_2O molecules. The H_2O fluids in illite-8K^+-water pore space and in illite-8K^+-PMMA pore space are skewed to have a larger number of smaller angles. This result indicates that the dominant orientation of H_2O fluids is a vector pointing from each O atom to H atom both perpendicular to the illite surface and pointing away from the illite surface. This orientation is depicted in Figure 19. This orientation is indicative of the effect of the K^+ ions at the surface of the illite on the H_2O molecules. This surface is hydrophilic and the H_2O molecules orient themselves so that the negative dipoles point towards the K+ ions. This interaction between the fluids and the illite surface create a higher interfacial energy between illite-8K^+-water and H_2O fluid than between the illite-0K^+-water and $scCO_2$ fluid (0.04160 J/m^2 vs 0.00206 J/m^2). Surprisingly, the illite-8K+-PMMA does not create this same disparity between interfacial tensions. In fact, $scCO_2$ fluid has a much higher interfacial tension with illite-8K^+-PMMA than water does with the surface (0.01344 J/m^2 vs 0.00088 J/m^2). This anomaly shows the degree to which the PMMA monolayer influences the interfacial tensions with fluid.

Figure 20 shows the ADF results for the models with CO_2 fluid, averaged for ≈5 picoseconds. The 25 CO_2 and 28 CO_2 models are centered at 90º. The CO_2 fluids in the pore space of illite-0K^+-water, illite-0K^+-PMMA, illite-8K^+-water, and illite-8K^+-PMMA also orient themselves centered at 90º. These results indicate that the CO_2 molecules are not affected by the presence of illite. The CO_2 fluids in illite-8K^+-water pore space have multiple high angle peaks because of oxalate compounds that form, which do not rotate as much in the pores. Unlike the H_2O fluid models, all of the CO_2 fluid models do not orient themselves parallel to the z-axis. This could be a result of symmetry of the model lattice. Because the z-axis is a much longer distance, the CO_2 molecules can minimize their energy between each other by orienting more perpendicular to the axis.

The structures of the models provide insight into the interfacial energies with the illite. The interfacial energy between H_2O and illite-0K^+-water was much lower than the interfacial energy between H_2O and illite-8K^+-water. This difference is because of the K^+ interacting with the negative dipoles in H_2O. The disparity between these interfacial energies (0.0111 vs 0.04222 J/m^2) shows the importance of the presence of K^+. In real clays, illite contains K^+ which would interact with water. Therefore, the interfacial energy between H_2O and illlite-8K^+-water is a more reasonable result. The presence of K^+ of illite has little effect on the CO_2 fluid in pore space because CO_2 is non-polar. Similar results would also be expected in other clays such as smectites that contain charged ion surfaces, such as Ca^{2+} or Na^+ surfaces. As shown in Figure 20, the orientation of the CO_2 molecules do not change between the illite-0K^+-water and the illite-8K^+-water models. As a result, the interfacial tensions between CO_2 and these illite models are mostly similar (0.0126 vs 0.0220 J/m^2). The interfacial tension between CO_2 fluid and illite-8K^+-water could be due to the oxalate compound near the edge of the pores. The K^+ ion may have an

influence on forming oxalate but it is known if this occurs because of the modeling method employed, or if it would happen experimentally. Simulations where the oxalate formed were repeated with different starting configurations and the oxalate formed each time. If it is a result of the modeling method employed, than the interfacial tension between CO_2 and illite-8K^+-water would likely be lower. Further investigation by experimental and computational means would be beneficial.

The illite-PMMA models provide more inconclusive results. The interactions between the fluids and illite-PMMA surfaces consistently provide lower interfacial tensions, indicating that the PMMA molecule repels the fluids. The PMMA monolayer was added to the model to simulate hydrocarbons. Like hydrocarbons, PMMA is a hydrophobic, carbon-rich surface. It is unclear whether the PMMA molecules in this simulation is how the real-world system will work. Sc-CO_2 would be expected to be miscible with hydrocarbons in shale pores, further leading to a larger fracture network. This miscibility is not accurately modelled by this system. Overall, PMMA in the system may not be a reliable model for hydrocarbons in the system, and the results for these interfacial tensions are not as meaningful as the interactions with the illite-water surfaces.

4.5 Root-mean-squared displacement analysis

Table 6 shows the root-mean-squared displacement (RMSD) calculations for each of the models.

Model	25 CO_2	28 CO_2	CO_2 in illite-$8K^+$ -water-pore space	CO_2 in illite-$0K^+$ -water-pore space	$49H_2O$	$54H_2O$	H_2O in illite-$8K^+$ -water-pore space	H_2O in illite-$0K^+$ -water-pore space
Diffusion coefficient (x 10^{-5} cm^2/s)	1.57	1.55	0.72	1.38	1.19	1.18	1.03	1.24

Model	CO_2 in illite-$8K^+$-PMMA-pore space	CO_2 in illite-$0K^+$ -PMMA-pore space	H_2O in illite-$8K^+$-PMMA-pore space	H_2O in illite-$0K^+$-PMMA-pore space
Diffusion coefficient (x 10^{-5} cm^2/s)	12.3	11.6	7.13	6.27

Table 6: Root-mean-squared displacement analysis results for fluids

For the models with CO_2 fluid, the illite-$8K^+$-water significantly slows down the movement of the H_2O molecules due to the interaction between the H_2O dipole and K^+ ions. These results, however, are inconclusive from the RMSD calculations because of the high degree of uncertainity in our relatively short MD simulations.

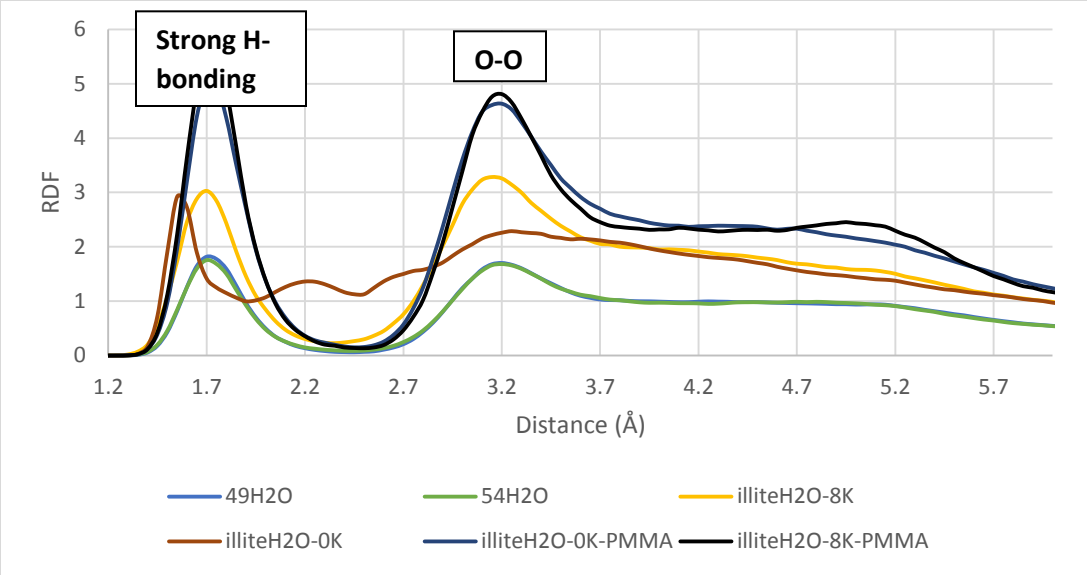

Figure 15: Radial distribution function results for models with H_2O fluid

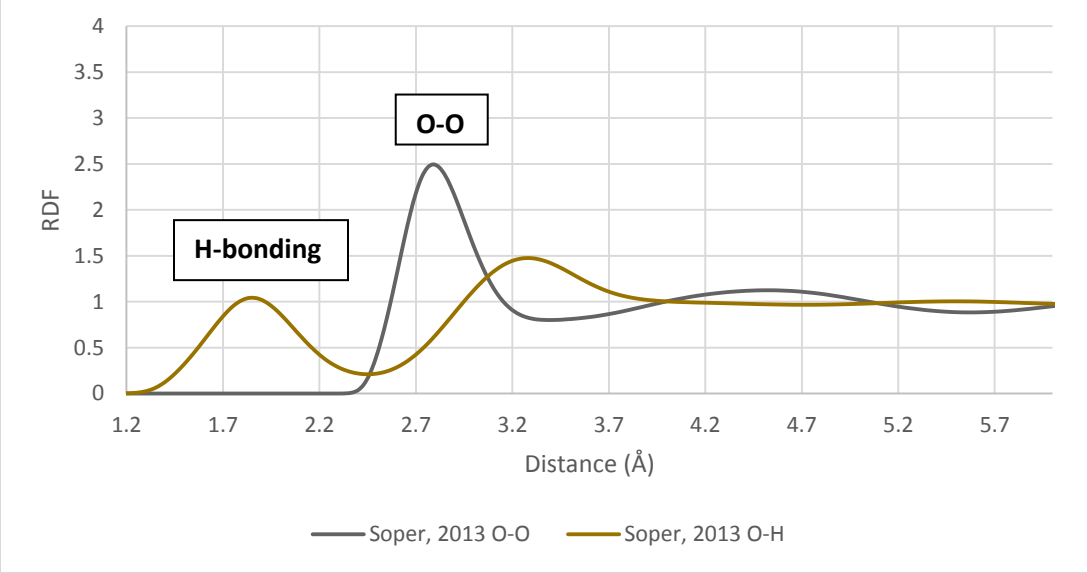

Figure 16: Radial distribution function results for models with H_2O molecules from Soper (2013)

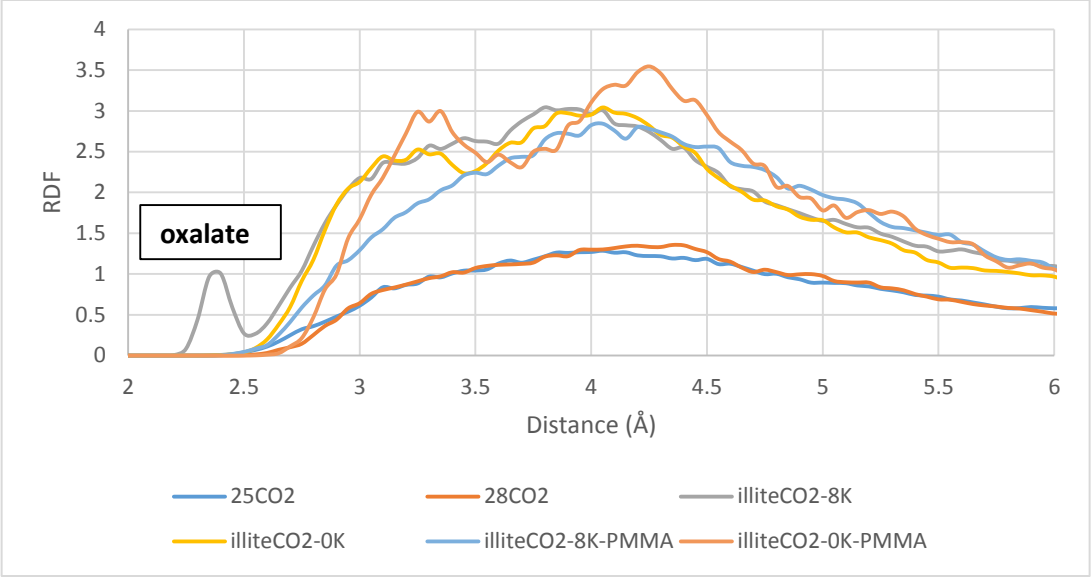

Figure 17: Radial distribution function results for models with CO_2 fluid

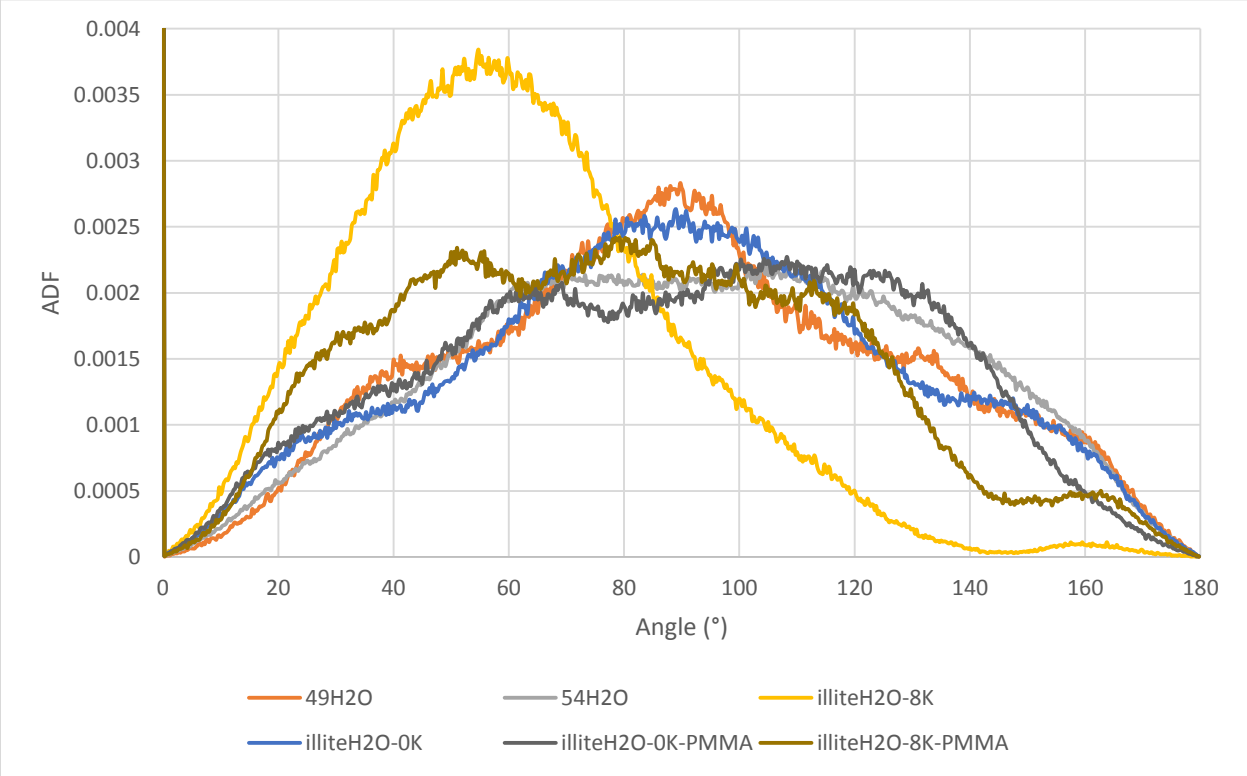

Figure 18: Angular distribution function results for models with H_2O fluid

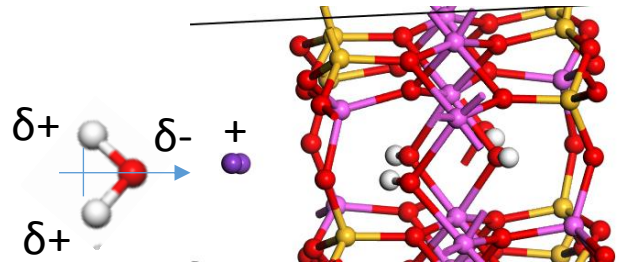

Figure 19: Dominant dipole orientation in illite-8K$^+$-water with H_2O fluid model as shown by ADF results

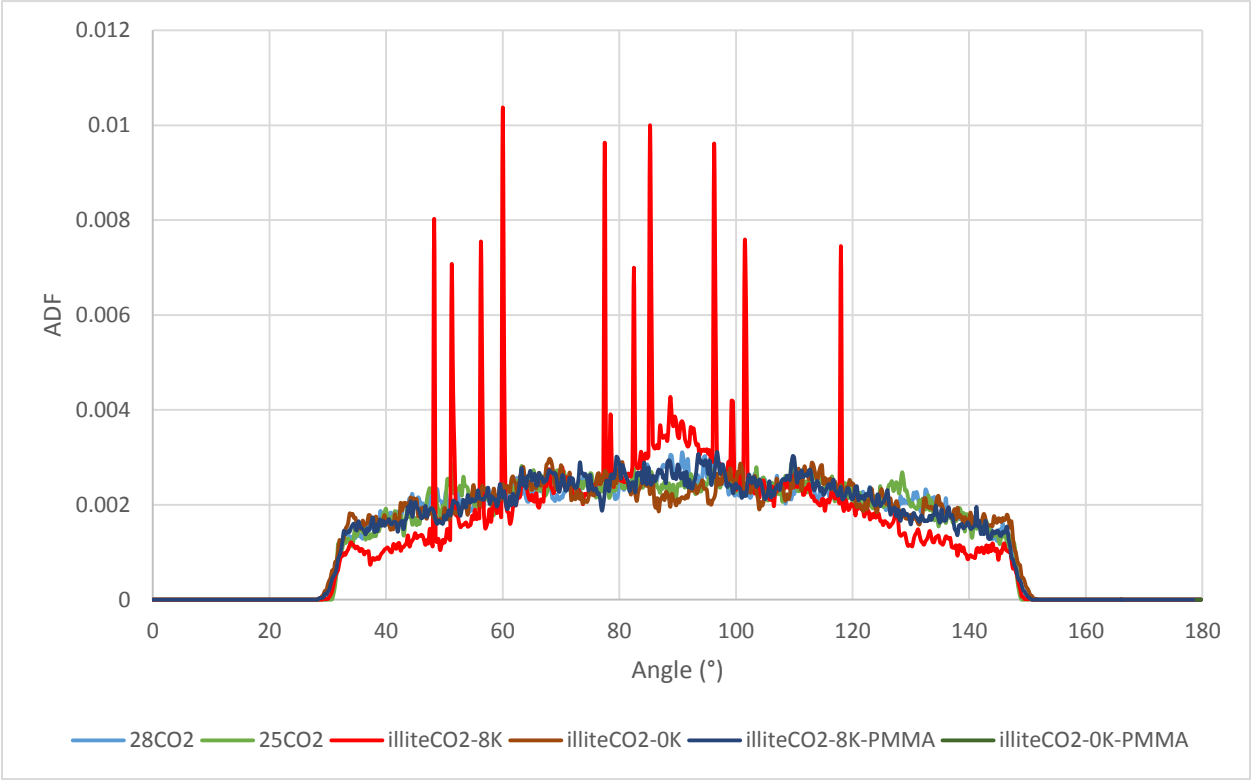

Figure 20: Angular distribution function results for models with CO_2 fluid

5.0 CONCLUSIONS

5.1 Summary of results

Supercritical CO_2 creates a lower interfacial tension with illite than water does with illite. For the illite-0K^+-water model, the CO_2-illite interfacial tension was 0.01261 J/m^2 and the H_2O-illite interfacial tension was 0.01112 J/m^2. For the illite-8K^+-water model, the CO_2-illite interfacial tension was 0.02198 J/m^2 and the H_2O-illite interfacial tension was 0.04220 J/m^2. All of the interfacial tensions are in a range comparable with experimental results (Dickson et al., 2006), (Espinoza et al., 2010). The interfacial tensions with the illite-PMMA surfaces are less conclusive.

The RDF results indicate that for most of the models, the distances between fluid molecules are not affected by the presence of illite. However for the illite-0K^+-water with H_2O fluid model depicted in Figure 27, there is an additional peak at 2.2 Å indicating weak hydrogen bonding. This peak is created by the hydrophobic illite surface.

The ADF results in Figures 30 and 32 indicate that the H_2O fluids in illite-0K^+-water pore space and CO_2 fluids in illite-0K^+-water pore space are not affected by the presence of the surface. Figure 30 shows that the illite-8K^+-water model skews the H_2O fluids to lower angles. This indicates that the water molecules are forming dipoles in response to the K^+ ions with vectors from the O to H atoms pointing away or perpendicular to the illite. The illite-8K^+-water model also affects the CO_2 fluids by causing a complex to form near the edge of the pores. It is unknown whether this occurs due to the molecular modeling methods employed. The interaction between the illite-8K^+-water models and both of the fluids causes the interfacial tensions to be higher than between the illite-0K^+-water models and fluids. The interaction between H_2O and

illite-$8K^+$-water is much more significant than the interactions between CO_2 and illite-$8K^+$-water, resulting in a higher interfacial tension. (0.04220 J/m^2 vs 0.02198 J/m^2).

The RMSD results show that the illite-$8K^+$-water might slow down the diffusion of H_2O molecules.

5.2 Implication for fluid-rock interaction and hydraulic fracturing

$ScCO_2$ has a smaller interfacial tension with illite than water does with illite. As a result, as a hydraulic fracturing fluid, $scCO_2$ could seep into the nanopores of illite at lower pressures and create fractures with a larger surface area. A larger volume of hydrocarbons could then be extracted from the shale. Consequently, $scCO_2$ would act as a more effective hydraulic fracturing fluid and could replace water. Also, companies could would be able to take advantage of infrastructure to capture and transport CO_2 that could be created if carbon sequestration was more widely implemented. Finally, $scCO_2$ could be used in areas that are hesitant to use hydraulic fracturing because of the expense of water.

5.3 Possible cautions in using $scCO_2$ as a hydraulic fracturing fluid

There are a number of factors beyond the scope of this study that could discourage the use of $scCO_2$ as a hydraulic fracturing fluid. $ScCO_2$ may lack the ability to carry proppants deeper underground, so might only be useful hydrofracturing at shallower depths. Proppants are very important in keeping a hydraulic fracture open so that the hydrocarbons are extracted. Companies are working on determining the best viscosity to maximize $scCO_2$'s abiliity to carry proppants (*Topf, 2014*). Also, $scCO_2$ can be difficult to transport efficiently through existing pipelines (*McClung et al., 2012*). Pressure drops across valves in the pipelines must be controlled very carefully, to avoid phase changes in the CO_2; rapid phase changes can lead to freezing components, inhibiting transport (*McClung et al., 2012*). Also, if too much water is in the $scCO_2$,

it will create corrosion and hydrate formation, inhibiting transport of medium (*McClung et al., 2012*).

5.4 Future considerations

There are a number of addition molecular modeling studies that can be performed to further test the findings of this study. This study models fluid initially entering the pores of the illite. Additional models can be built to show fluid pressure building up in the pores of the illite, to calculate the amount of pressure needed to eventually cause the illite to fracture open. This could be acomplished using the same methods of this study by adding more molecules of fluid to the pore space. Alternatively, models can be built with various sizes of pore space of illite.

Molecular modeling studies could also be employed to address the cautions stated earlier in using $scCO_2$ as a fracturing fluid. In the past, it has been assumed that $scCO_2$ has lower proppant transport capacity (*Gensterblum et al., 2015*). A researcher could use quartz to model a proppant in the $scCO_2$ and study its motion through a lattice. This could help oil companies understand the molecular interactions involved to help improve $scCO_2$'s ability to carry proppants. In our study, the illite-PMMA did not yield very useful results. Further research could be employed to find if a better surface can be used to simulate hydrocarbon-filled pores of illite, to better see how the fluids would interact with the hydrocarbons. Methane could be a good compound to model into the pores of illite, that may behave more like natural gas.

There is also considerable potential in employing different molecular modeling methods to conduct the same research. For this study, we employed molecular dynamics simulations, which assigns force fields to individual atoms to yield energies of a system. The modeling could be repeated on a mesoscale in which force fields are applied to each different fluid molecule, a proccess called dissipative particle dynamics (DPD) (*Moeendarbary et al. 2009*). This modeling

technique is often employed for fluid molecules (*Moeendarbary et al. 2009*). Like MD simulations, it would also parameterize N, V, and T and find energy over a period of time.

6.0 REFERENCES

Alpern, Jennifer S. (2013) The influence of fluid properties on geometric complexity and breakdown pressure on hydraulic fracture. M.S. Thesis, Pennsylvania State University.

Arthur D. J. and Langhus B. P. G. (2008) An overview of modern shale gas development in the United States. *ALL Consult.*, 1–21. Available at: http://www.all-llc.com/publicdownloads/ALLShaleOverviewFINAL.pdf.

Bacon, D. H., Yonkofski, C. M. R., Schaef, H. T., White, M. D., & Mcgrail, B. P. (2015). Journal of Unconventional Oil and Gas Resources CO 2 storage by sorption on organic matter and clay in gas shale. *Journal of Unconventional Oil and Gas Resources*, *12*, 123–133. http://doi.org/10.1016/j.juogr.2015.09.004

Bao K., Yan M., Lu L., Allen R., Salama A., Jordan K. E. and Sun S. (2013) High-Performance Modeling of CO_2 Sequestration by Coupling Reservoir Simulation and Molecular Dynamics. *Proc. 2013 SPE Reserv. Simul. Symp.*, 163621–MS. Available at: http://www.onepetro.org/mslib/servlet/onepetropreview?id=SPE-163621-MS.

Blöchl P. E. (1994) Projector augmented-wave method. *Phys. Rev. B* **50**, 17953–17979.

Botan A., Rotenberg B., Marry V., Turq P. and Noetinger B. (2010) Carbon Dioxide in Montmorillonite Clay Hydrates: Thermodynamics, Structure, and Transport from Molecular Simulation. *J. Phys. Chem. C* **114**, 14962–14969. Available at: http://pubs.acs.org/doi/abs/10.1021/jp1043305.

Brantley, Susan L., Kathy Brasier, Chuck Anderson, Candie Wilderman, Julie Vastine, Jorge Abad, Radisav Vidic, and Rick Hooper. "The ShaleNetwork Database." *The ShaleNetwork Database*. ShaleNetwork.org, 19 Dec. 2011. Web. 18 Nov. 2014.

Busch, A., Alles, S., Gensterblum, Y., Prinz, D., Dewhurst, D. N., Raven, M. D., … Krooss, B. M. (2008). Carbon dioxide storage potential of shales, *2*, 297–308. http://doi.org/10.1016/j.ijggc.2008.03.003

Cygan R. T. (2001) Molecular Modeling in Mineralogy and Geochemistry. *Rev. Mineral. Geochemistry* **42**, 1–35. Available at: http://rimg.geoscienceworld.org/content/42/1/1.short

Cygan R. T., Romanov V. N. and Myshakin E. M. (2012) Molecular simulation of carbon dioxide capture by montmorillonite using an accurate and flexible force field. *J. Phys. Chem. C* **116**, 13079–13091.

McClung A., Moore J., Lerche A. and Morgan K. (2012) Pipeline Transport of Supercritical Carbon Dioxide. , 1–8.

Del Ben M., Hutter J. and VandeVondele J. (2015) Probing the structural and dynamical properties of liquid water with models including non-local electron correlation. *J. Chem. Phys.* **143**, 054506. Available at: http://scitation.aip.org/content/aip/journal/jcp/143/5/10.1063/1.4927325.

Dickson J. L., Gupta G., Horozov T. S., Binks B. P. and Johnston K. P. (2006) Wetting phenomena at the CO_2/water/glass interface. *Langmuir* **22**, 2161–2170.

Espinoza D. N. and Santamarina J. C. (2010) Water-CO_2-mineral systems: Interfacial tension, contact angle, and diffusion. Implications to CO_2 geological storage. *Water Resour. Res.* **46**, 1–10.

Galbraith, Kate. "Waterless Fracking Makes Headway in Texas, Slowly." Texas RSS. N.p., 27 Mar. 2013. Web. 03 Nov. 2014.

Gensterblum, Y., Ghanizadeh, A., Cuss, R. J., Amann-hildenbrand, A., Krooss, B. M., Clarkson, C. R., … Zoback, M. D. (2015). Journal of Unconventional Oil and Gas Resources Gas transport and storage capacity in shale gas reservoirs – A review . Part A : Transport

processes. *Journal of Unconventional Oil and Gas Resources*, *12*, 87–122. http://doi.org/10.1016/j.juogr.2015.08.001

Grimme S., Antony J., Ehrlich S. and Krieg H. (2010) A consistent and accurate ab initio parametrization of density functional dispersion correction (DFT-D) for the 94 elements H-Pu. *J. Chem. Phys.* **132**.

Heller, R., & Zoback, M. (2014). Journal of Unconventional Oil and Gas Resources Adsorption of methane and carbon dioxide on gas shale and pure mineral samples. *JOURNAL OF UNCONVENTIONAL OIL AND GAS RESOURCES*, *8*, 14–24. http://doi.org/10.1016/j.juogr.2014.06.001

Hester, R.E. and Harrison R.M. (2014) Fracking. *S.l.: Royal Soc Of Chemistry*. pp. 181-198.

Hosterman, J. W. and Whitlow, S.I. (1923) Clay Mineralogy of Devonian Shales in the Appalachian Clay Mineralogy of Devonian Shales in the Appalachian Basin.

Ishida T., Aoyagi K., Niwa T., Chen Y., Murata S., Chen Q. and Nakayama Y. (2012) Acoustic emission monitoring of hydraulic fracturing laboratory experiment with supercritical and liquid CO_2. *Geophys. Res. Lett.* **39**, L16309. Available at: http://dx.doi.org/10.1029/2012GL052788.

Ishida T., Chen Q., Mizuta Y. and Roegiers J.-C. (2004) Influence of Fluid Viscosity on the Hydraulic Fracturing Mechanism. *J. Energy Resour. Technol.* **126**, 190.

Jaynes W. F. and Boyd S. a. (1991) Hydrophobicity of siloxane surfaces in smectites as revealed by aromatic hydrocarbon adsorption from water. *Clays Clay Miner.* **39**, 428–436.

Jing, M. (2012) Breaking New Ground. *China Daily*.

Johnson E. and Cleary M. P. (1991) Implications of recent laboratory experimental results for hydraulic fractures. *Rocky Mt. Reg. Meet. Low-Permeability Reserv. Symp.*, 413–428.

Jones, R. O. and Gunnarsson, O. (1989). The density functional formalism, its applications and prospects. *Rev. Mod. Phys.*, *61*(3), 689–746. Retrieved from http://link.aps.org/doi/10.1103/RevModPhys.61.689

Khosrokhavar, R., Wolf, K., & Bruining, H. (2014). International Journal of Coal Geology Sorption of CH4 and CO2 on a carboniferous shale from Belgium using a manometric setup. *International Journal of Coal Geology*, *128-129*, 153–161. http://doi.org/10.1016/j.coal.2014.04.014

King G. E. (2012) Hydraulic Fracturing 101 : *SPE One Petro*, 1–80.

Kresse G. (1999) From ultrasoft pseudopotentials to the projector augmented-wave method. *Phys. Rev. B* **59**, 1758–1775.

LionX Systems — PSU ICS. (n.d.). Retrieved October 7, 2015.

Lockard, Gene. "Fracking Goes Waterless: Gas Fracking Could Silence Critics." *RIGZONE*. N.p., 26 Sept. 2013. Web. 18 Nov. 2014.

Ma, Wayne. "China's Shale-Gas Boom Slow to Start." *The Wall Street Journal*. Dow Jones & Company, 3 Dec. 2012. Web. 11 Nov. 2014.

Maverick, T. (2014) Key Players in the Shale Industry's Shift to Carbon Dioxide. *Wall Street Daily*.

McCaughan J., Iglauer S. and Bresme F. (2013) Molecular dynamics simulation of water/CO_2-quartz interfacial properties: Application to subsurface gas injection. *Energy Procedia* **37**, 5387–5402. Available at: http://dx.doi.org/10.1016/j.egypro.2013.06.457.

Miller C.C. (1924) The Stokes-Einstein Law for Diffusion in Solution. *Royal Society*. **106**, 724-29. Available at: http://www.jstor.org/stable/94335?seq=16#page_scan_tab_contents.

Milman, V., Winkler, B., White, J. A., Pickard, C. J., Payne, M. C. Akhmatskaya, E. V., & Nobes, R. H. (2000). Electronic structure, properties, and phase stability of inorganic crystals: A pseudopotential plane-wave study. *Int. J. Quantum Chem.*, *77*(5), 895–910.

Moeendarbary, E., NG, T. Y., & Zangeneh, M. (2009). DISSIPATIVE PARTICLE DYNAMICS: INTRODUCTION, METHODOLOGY AND COMPLEX FLUID APPLICATIONS — A REVIEW. *International Journal of Applied Mechanics*, *1*(4), 737–763.

Montgomery C. T. and Smith M. B. (2010) Hydraulic Fracturing History of an Enduring Technology. *JPT* **62**, 26–32. Available at: www.spe.org/jpt/print/archives/2010/12/10Hydraulic.pdf?

Papadopoulos J. M., Narendran V. M. and Cleary M. P. (1983) Laboratory Simulations of Hydraulic Fracturing. *SPE/DOE Symp. Low Permeability*, 161–168.

Payne, M. (2004) *Vienna Ab-initio Simulation Package*. Vers. 4.6. Computer software.

Payne, M. C., Teter, M. P., Allan, D. C., Arias, T. A., & Joannopoulos, J. D. (1992). Iterative minimization techniques for ab initio total-energy calculations: molecular dynamics and conjugate gradients. *Rev. Mod. Phys.*, *64*(4), 1045–1097. Retrieved from http://link.aps.org/doi/10.1103/RevModPhys.64.1045

Rao, Q., Xiang, Y., and Leng, Y. S., "Molecular simulations on the structure and dynamics of water-methane fluids between Na-Montmorillonite clay surfaces at elevated temperature and pressure," J. Phys. Chem. C, **117**, 14061 (2013)

Rappe A. K., Casewit C. J., Colwell K. S., Goddard III W. A. and Skiff W. M. (1992) UFF, a Full Periodic Table Force Field for Molecular Mechanics and Molecular Dynamics Simulations. *J. Am. Chem. Soc.* **114**, 10024–10035.

Schaef H. T., Glezakou V. -a., Owen a T., Ramprasad S., Martin P. F. and McGrail B. P. (2014) Surface Condensation of CO_2 onto Kaolinite. *Environ. Sci. Technol. Lett.* **1**, 142–145. Available at: http://pubs.acs.org/doi/abs/10.1021/ez400169b.

Sherman, D. M. (2016). Introduction to the Theory and Methods of Computational Chemistry.

Soper a. K. (2013) The Radial Distribution Functions of Water as Derived from Radiation Total Scattering Experiments: Is There Anything We Can Say for Sure? *ISNR Phys. Chem.* **2013**, 1.

Todd, S. (2013) *Materials Studio. Vers. 7.0.* Computer software.

Topf, Andrew. "Water-less Fracking Could be Industry Game Changer." OILPRICE.com. 6 Nov. 2014. Web. 1 Oct. 2016.

Wischneski, B. (2015) *Peace Software*. http://www.peacesoftware.de/.

Wright, R. (2010) Evaluating Reserves. *Wright and Company.*

VASP. 26 Mar. 2015. Wien, Austria: Kresse, G.; Marsman, M.; Furthmuller, J.

Verlet L. (1967) Computer "experiments" on classical fluids. I. Thermodynamical properties of Lennard-Jones molecules. *Phys. Rev.* **159**, 98–103

APPENDIX

$25CO_2$-MD

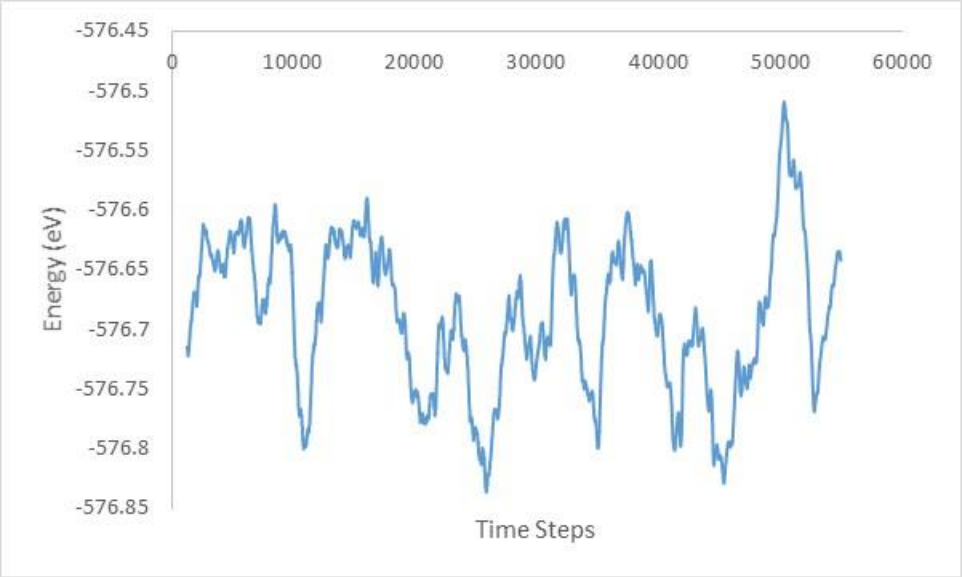

Energy vs time steps for MD simulations

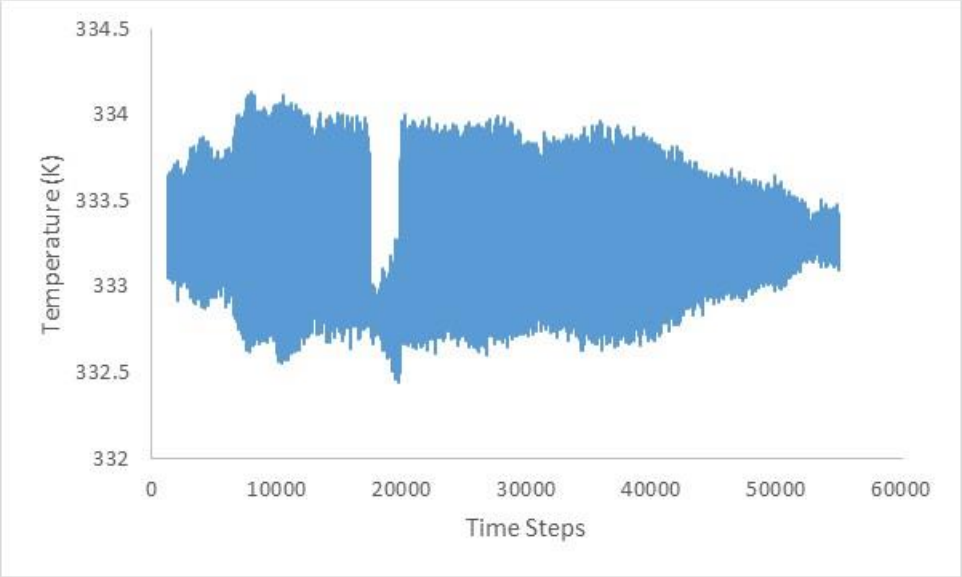

Temperature vs time steps for MD simulations

28CO_2-MD

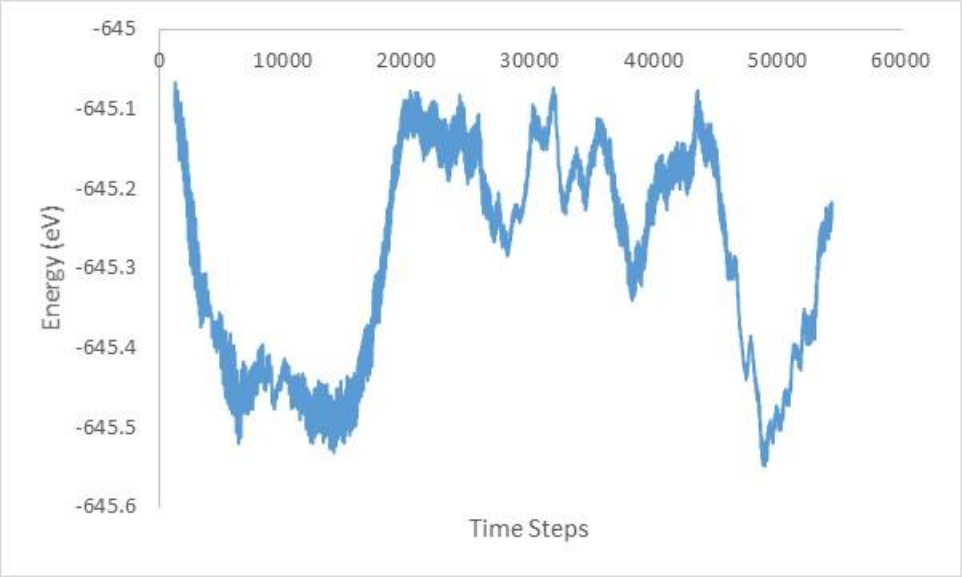

Energy vs time steps for MD simulations

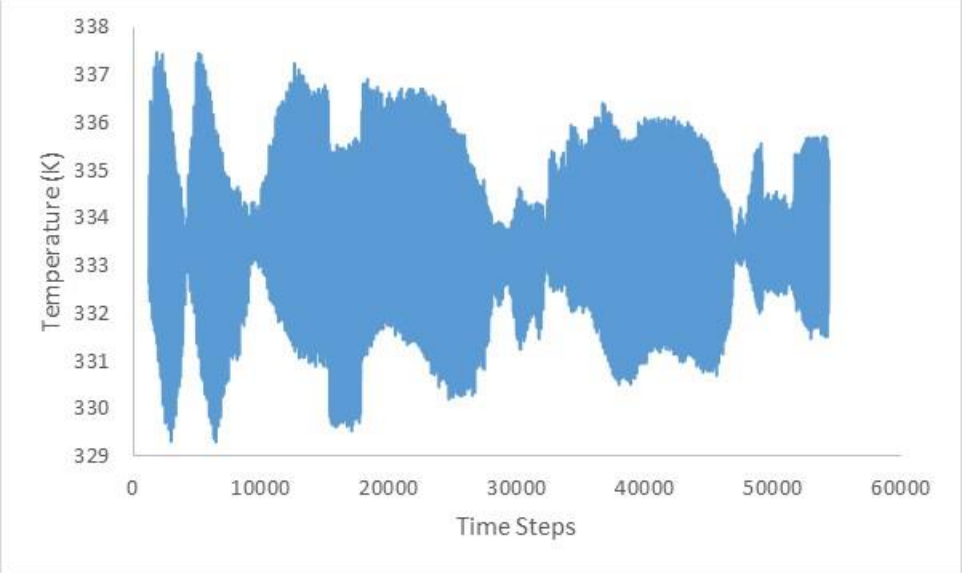

Temperature vs time steps for MD simulations

49H_2O-MD

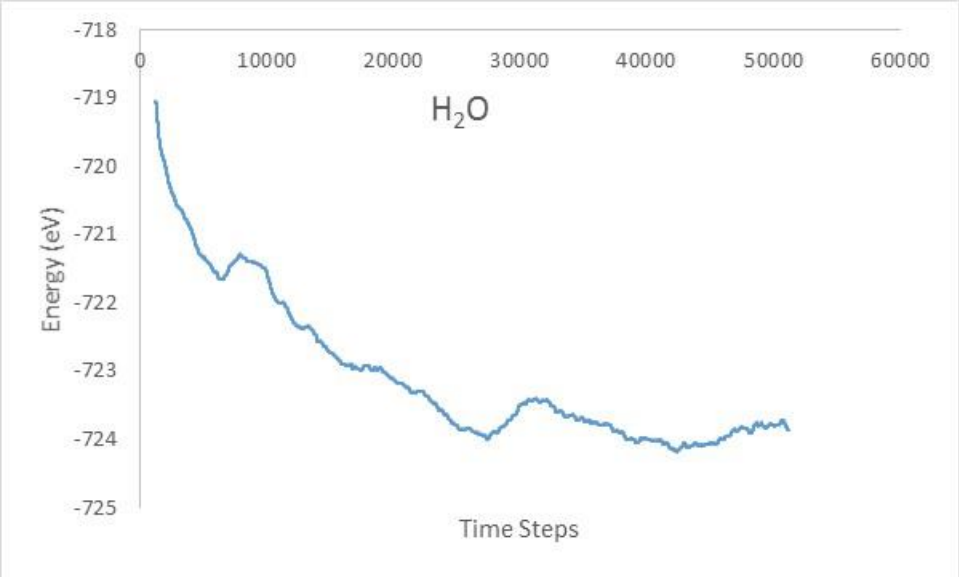

Energy vs time steps for MD simulations

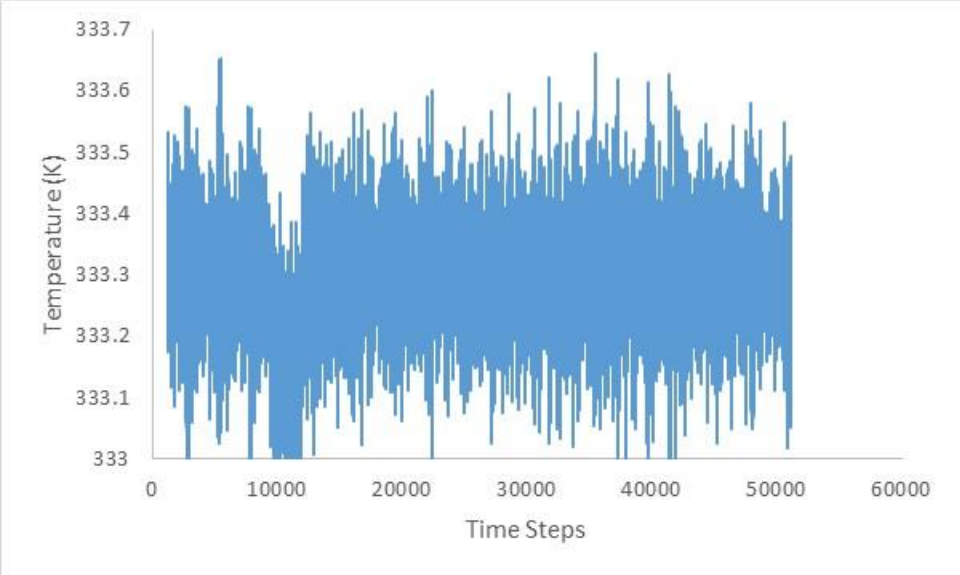

Temperature vs time steps for MD simulations

$54H_2O$-MD

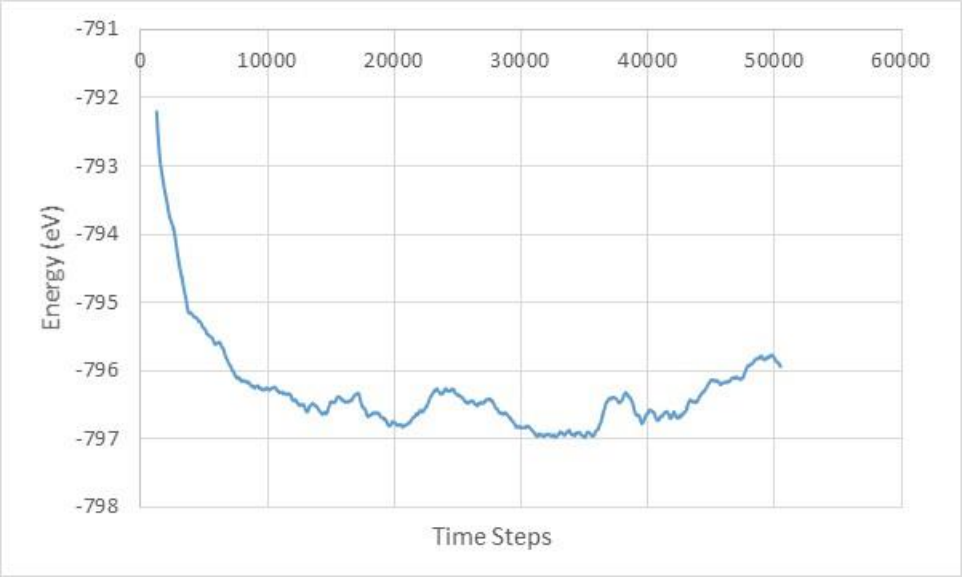

Energy vs time steps for MD simulations

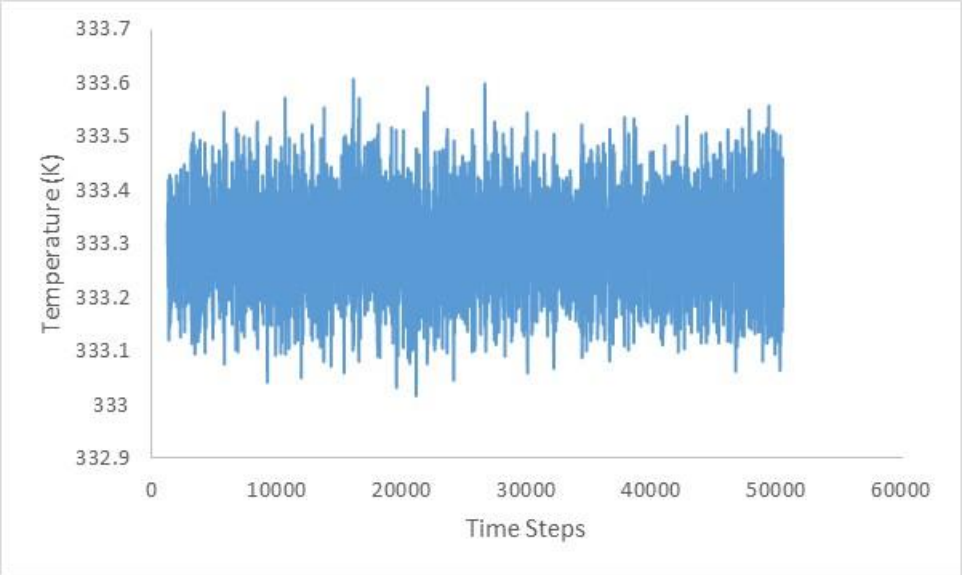

Temperature vs time steps for MD simulations

Illite-8K^+-water-MD

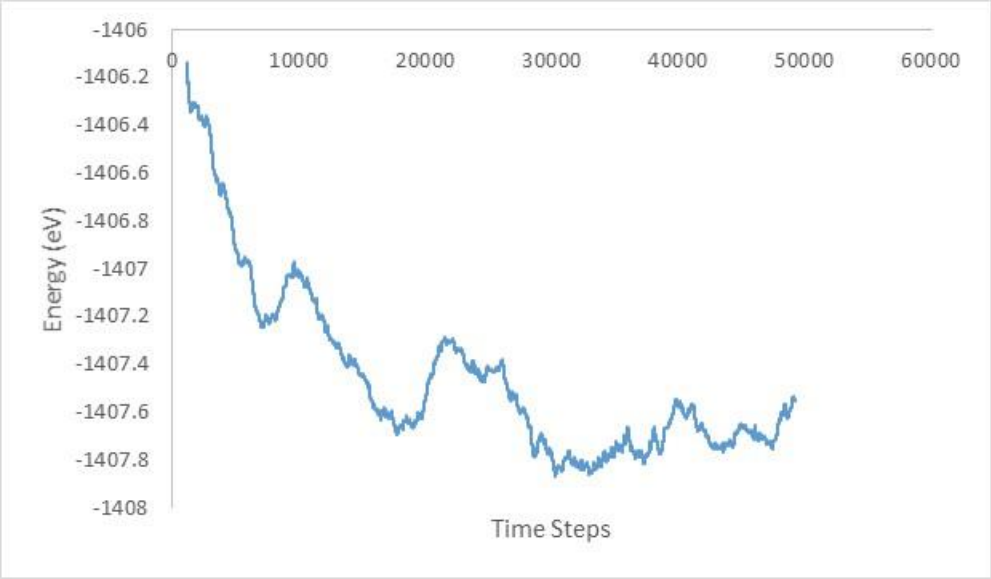

Energy vs time steps for MD simulations

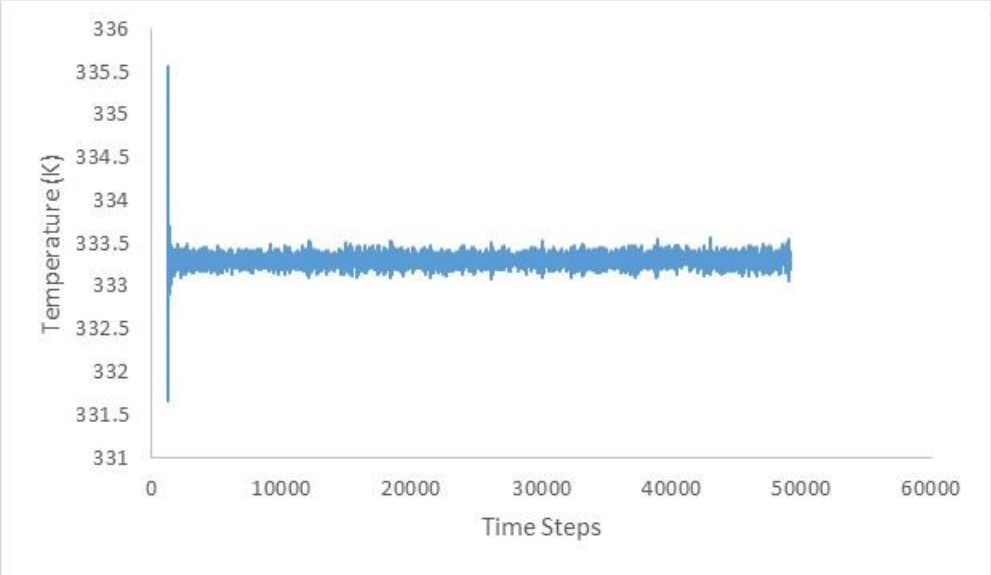

Temperature vs time steps for MD simulations

Illite-0K^+-water-MD

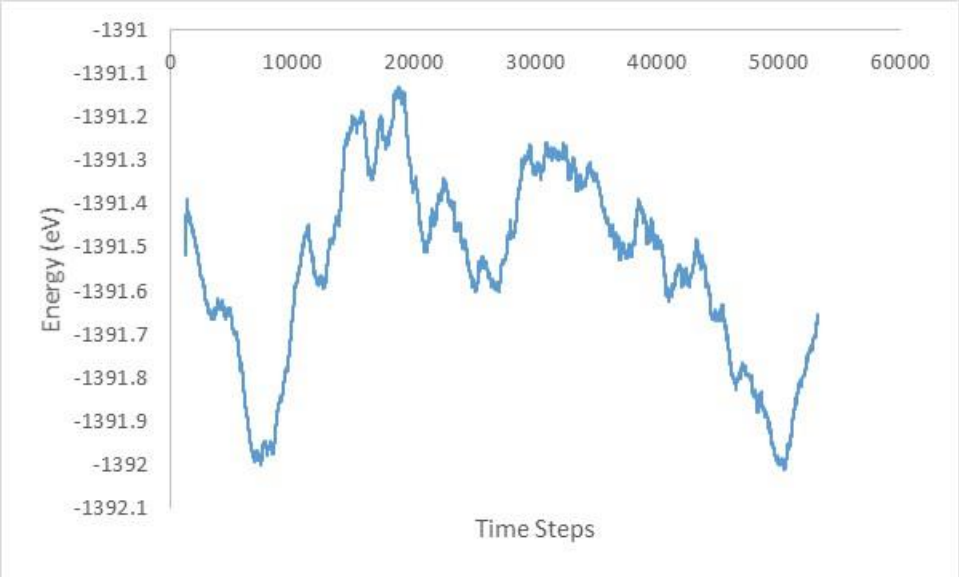

Energy vs time steps for MD simulations

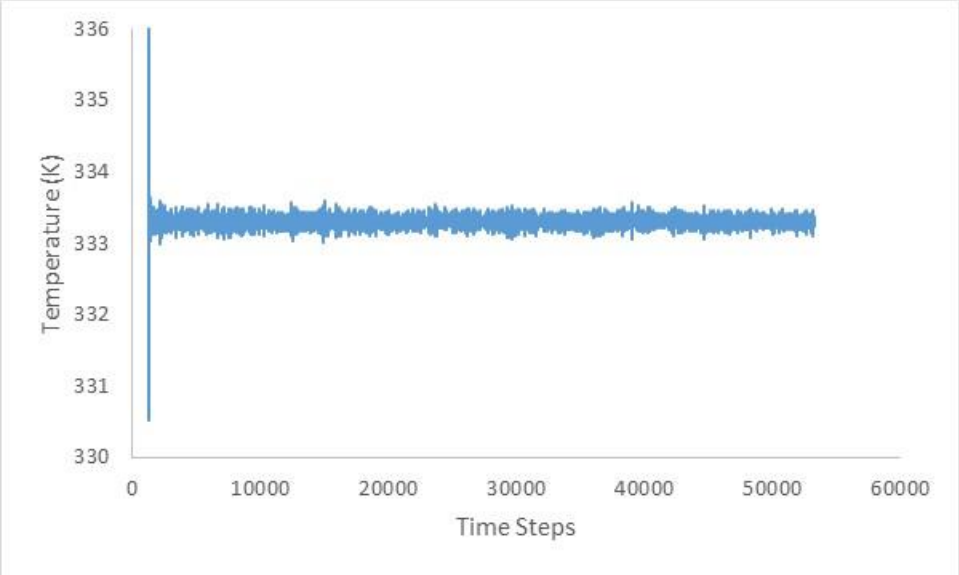

Temperature vs time steps for MD simulations

Illite-8K^+-PMMA-MD

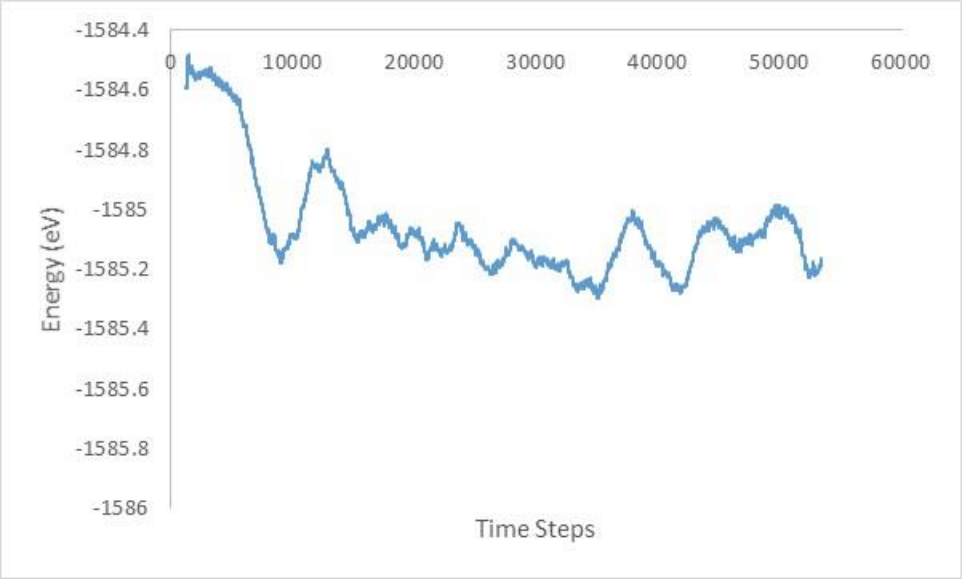

Energy vs time steps for MD simulations

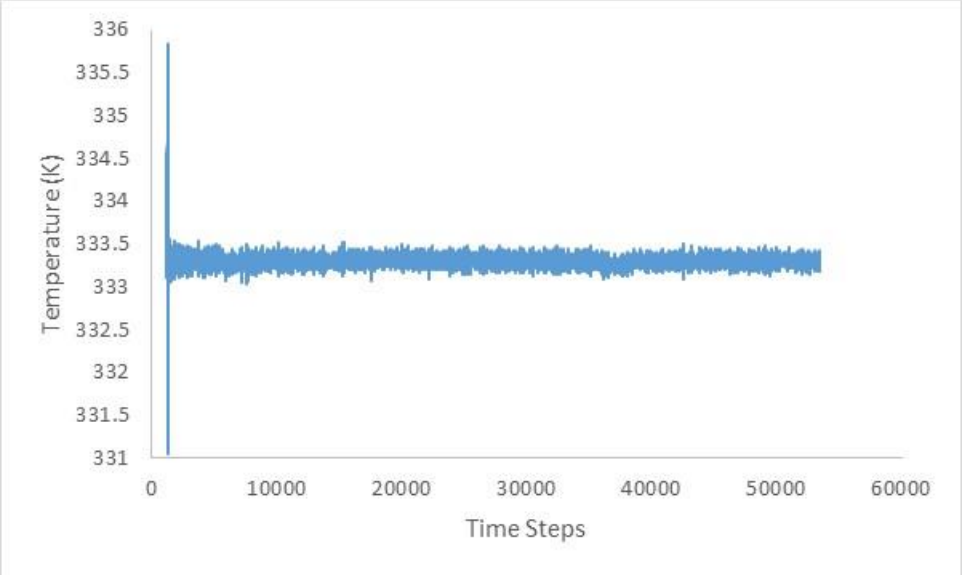

Temperature vs time steps for MD simulations

Illite-0K^+-PMMA-MD

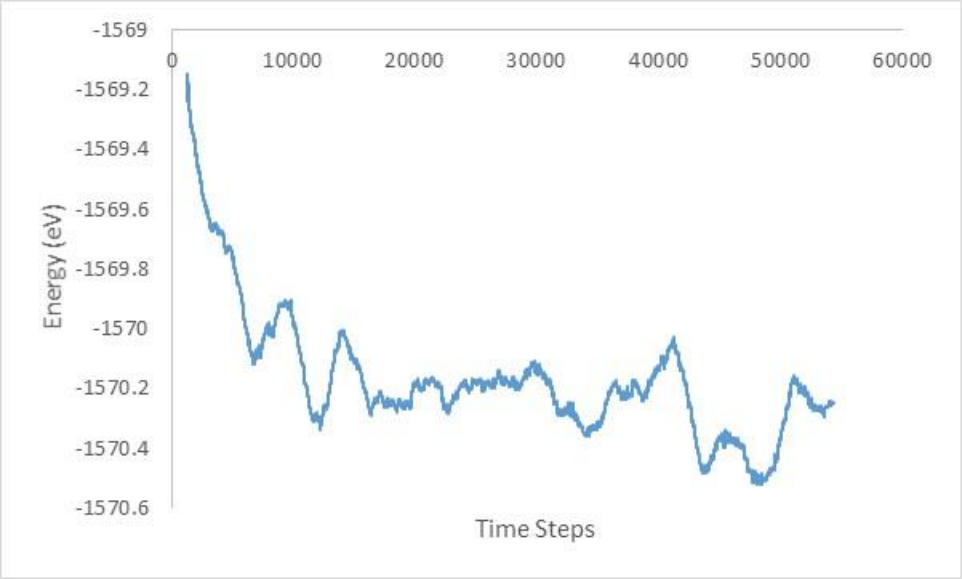

Energy vs time steps for MD simulations

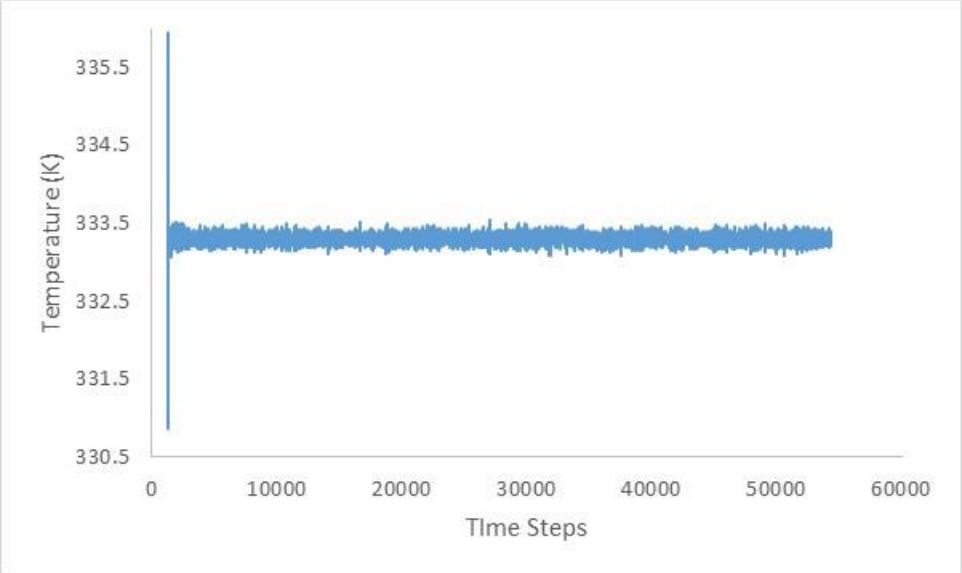

Temperature vs time steps for MD simulations

Illite-8K^+-water with H_2O in pore space-MD

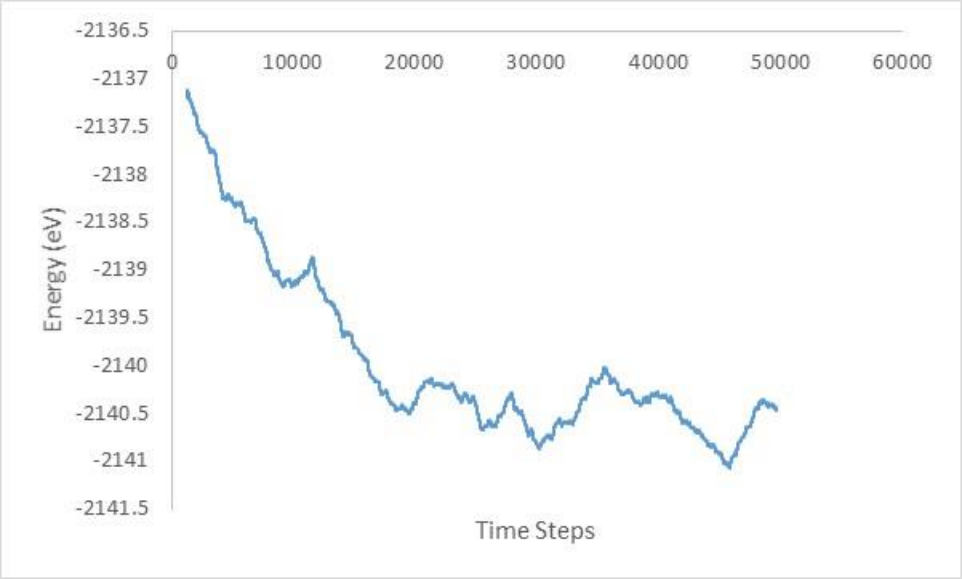

Energy vs time steps for MD simulations

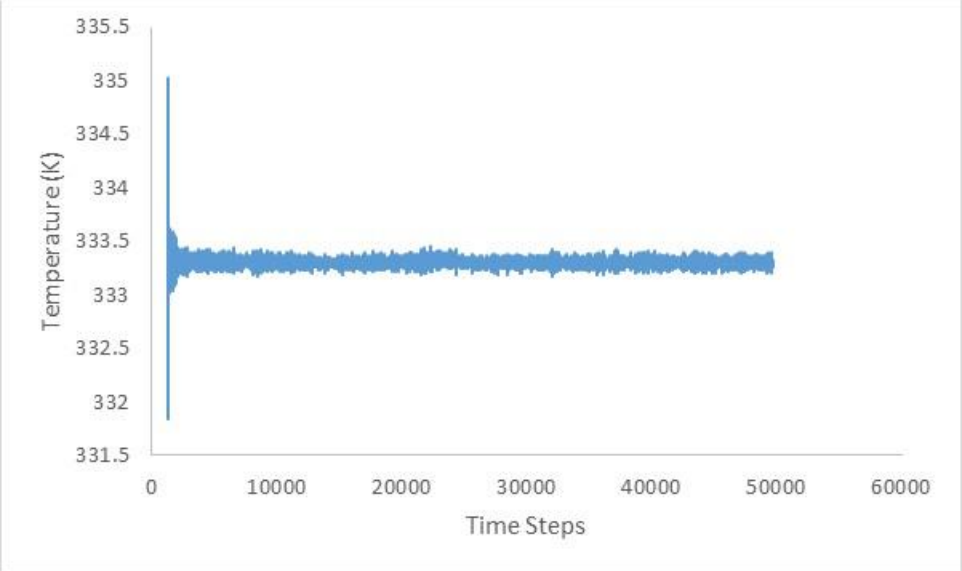

Temperature vs time steps for MD simulations

Illite-8K^+-water with CO_2 in pore space-MD

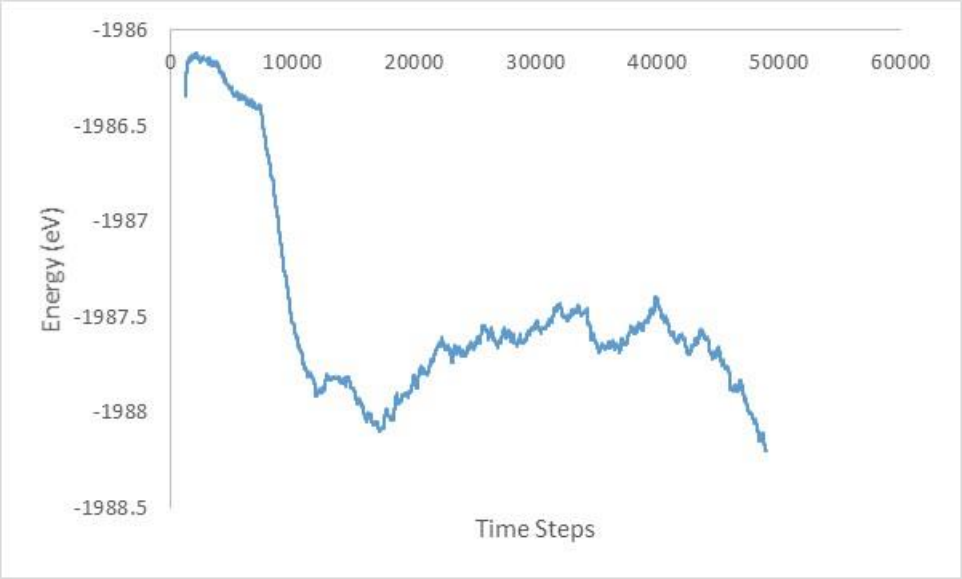

Energy vs time steps for MD simulations

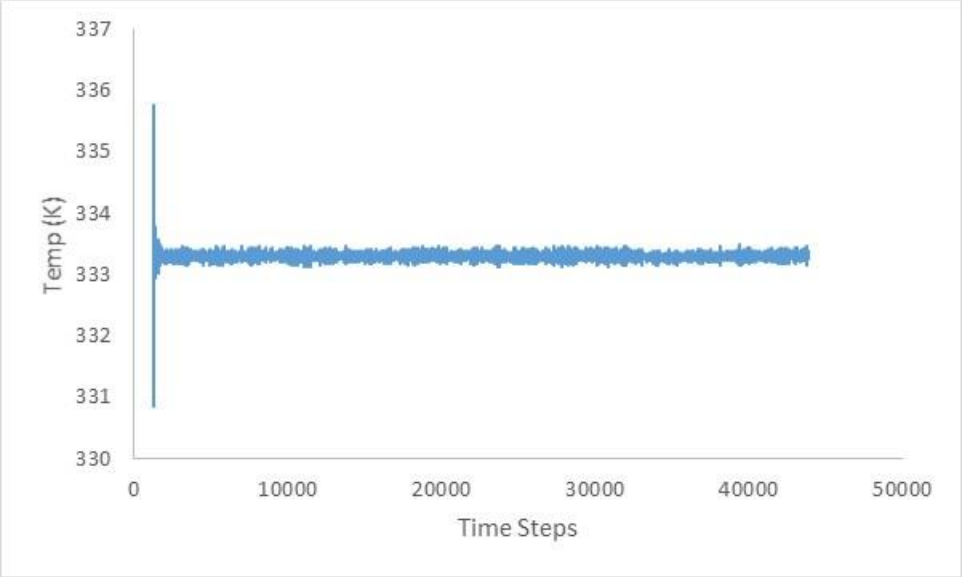

Temperature vs time steps for MD simulations

Illite-0K^+-water with H_2O in pore space-MD

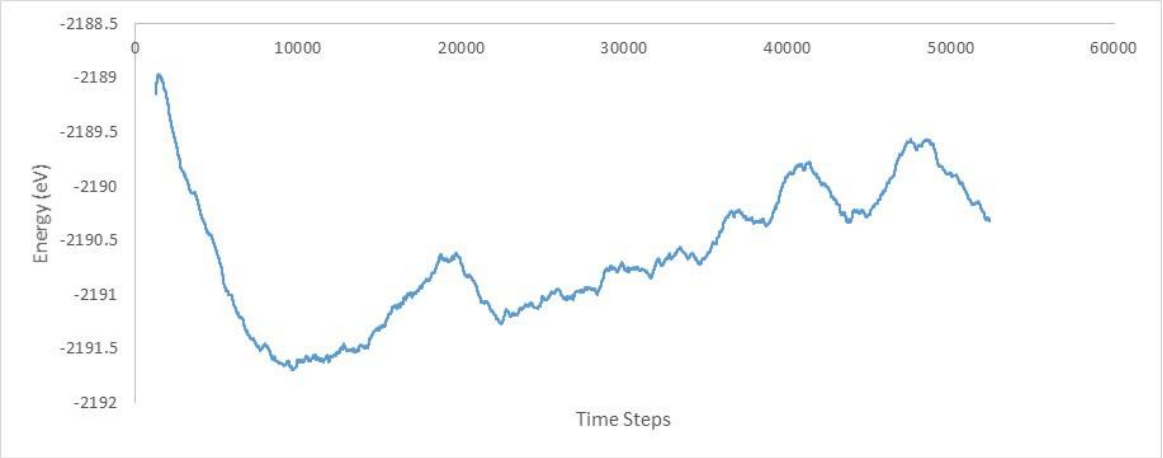

Energy vs time steps for MD simulations

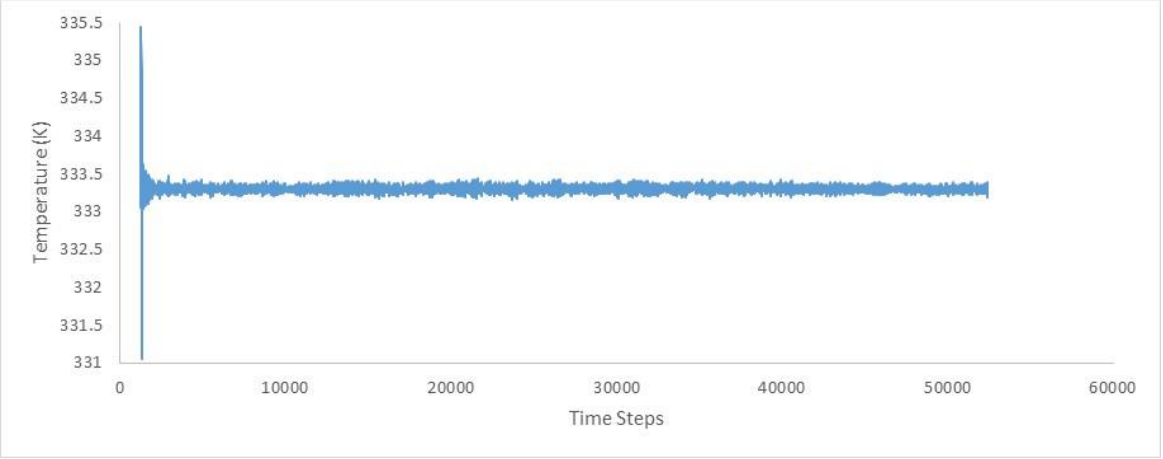

Temperature vs time steps for MD simulations

Illite-0K^+-water with CO_2 in pore space-MD

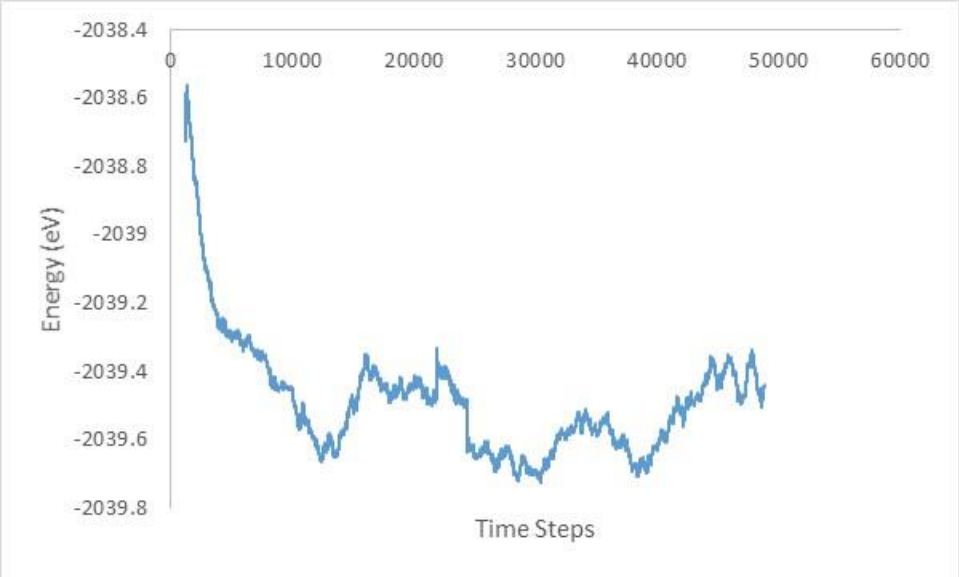

Energy vs time steps for MD simulations

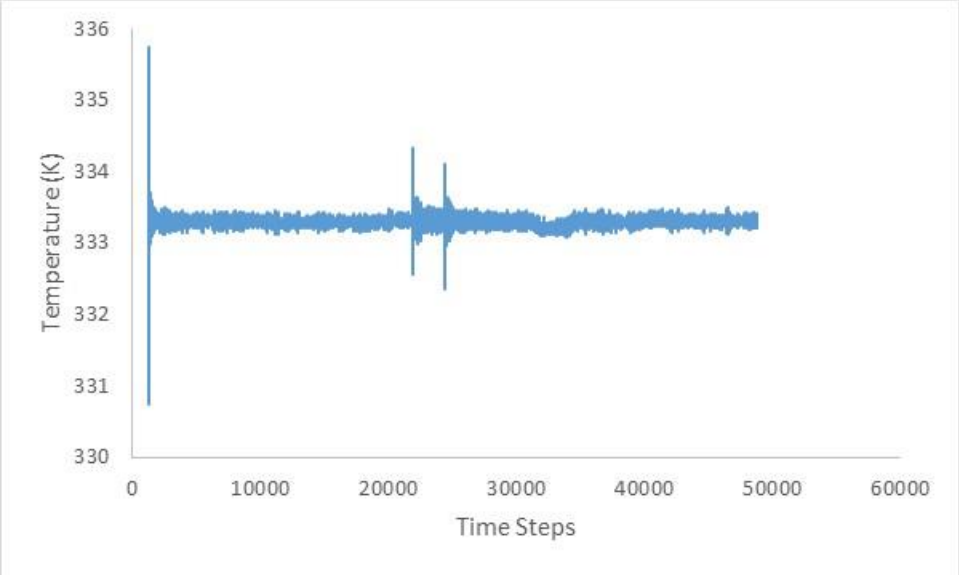

Temperature vs time steps for MD simulations

Illite-8K^+-PMMA with H_2O in pore space-MD

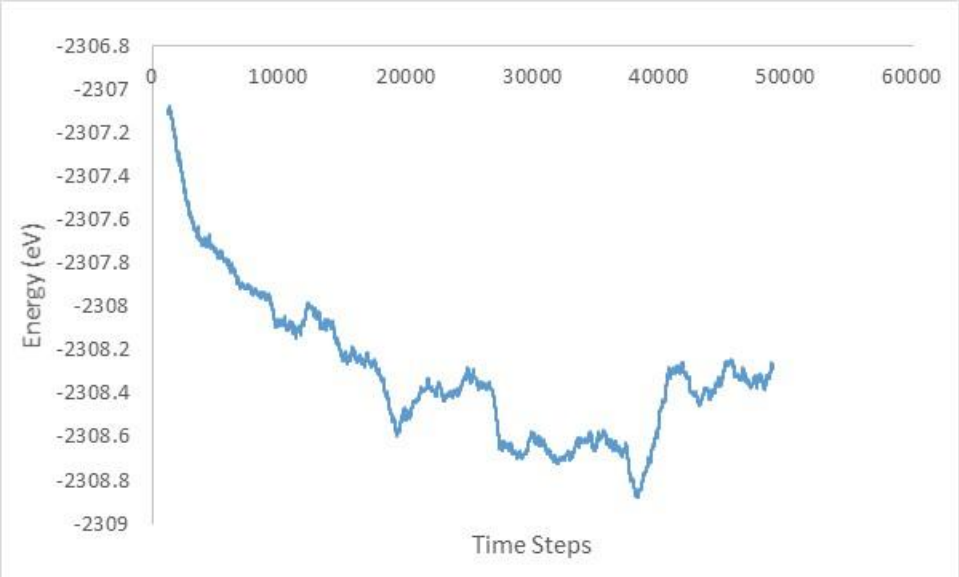

Energy vs time steps for MD simulations

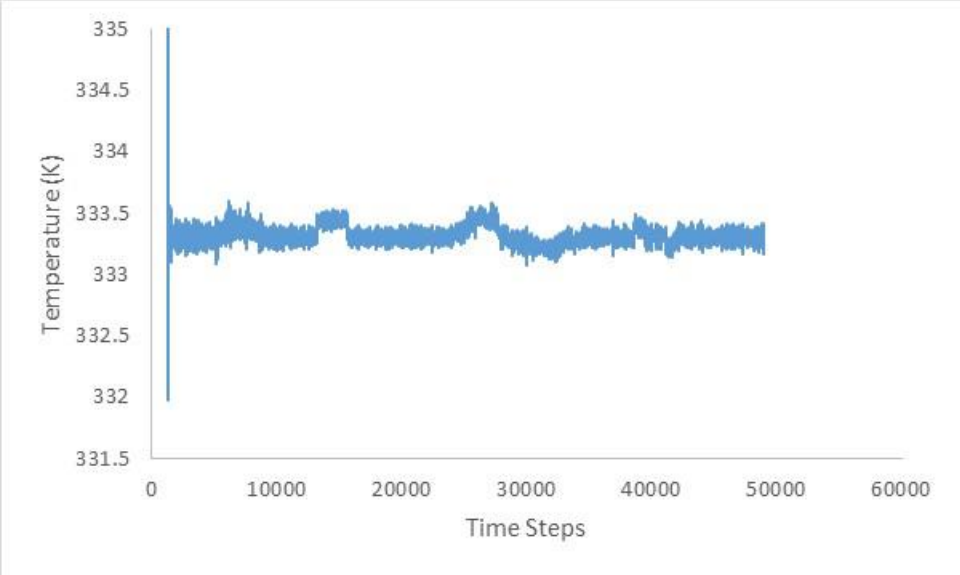

Temperature vs time steps for MD simulations

Illite-8K^+-PMMA with CO_2 in pore space-MD

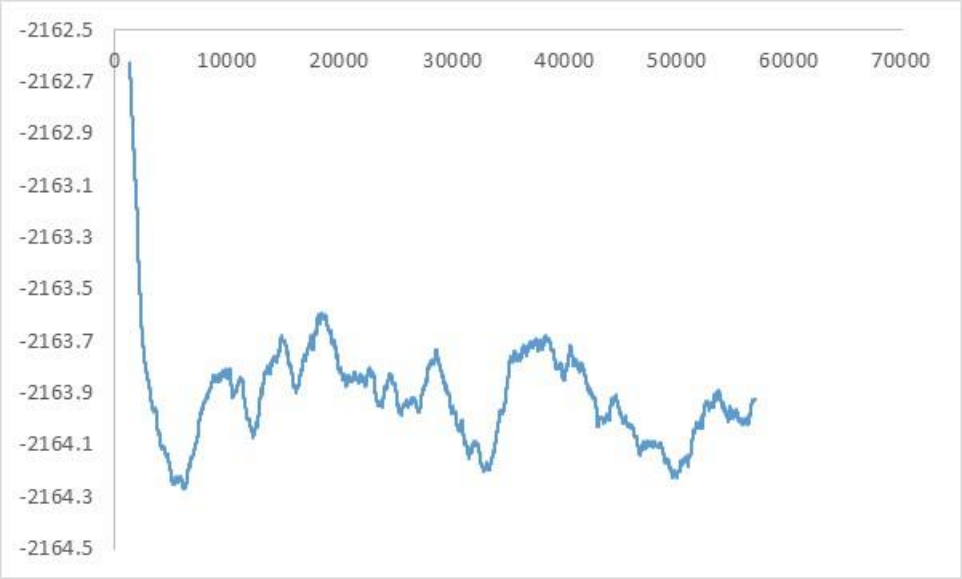

Energy vs time steps for MD simulations

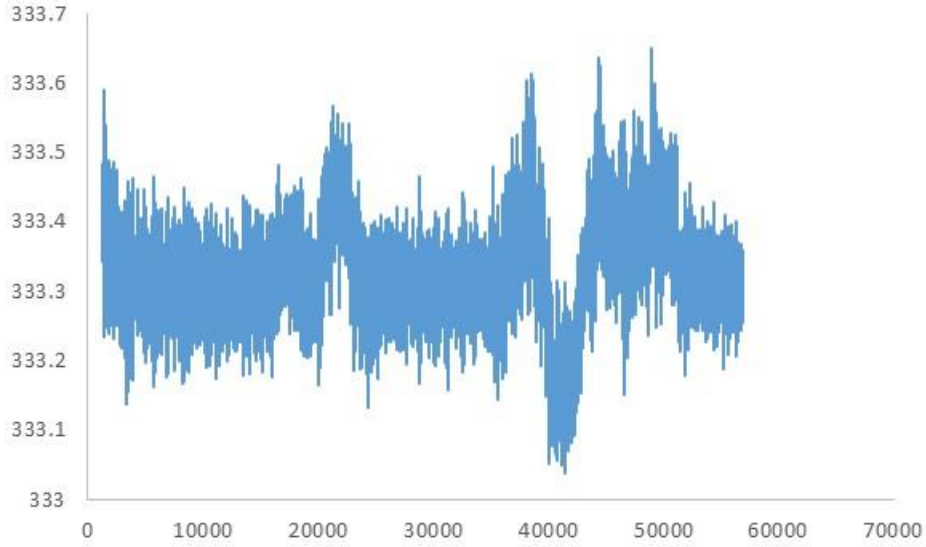

Temperature vs time steps for MD simulations

Illite-0K^+-PMMA with H_2O in pore space-MD

Energy vs time steps for MD simulations

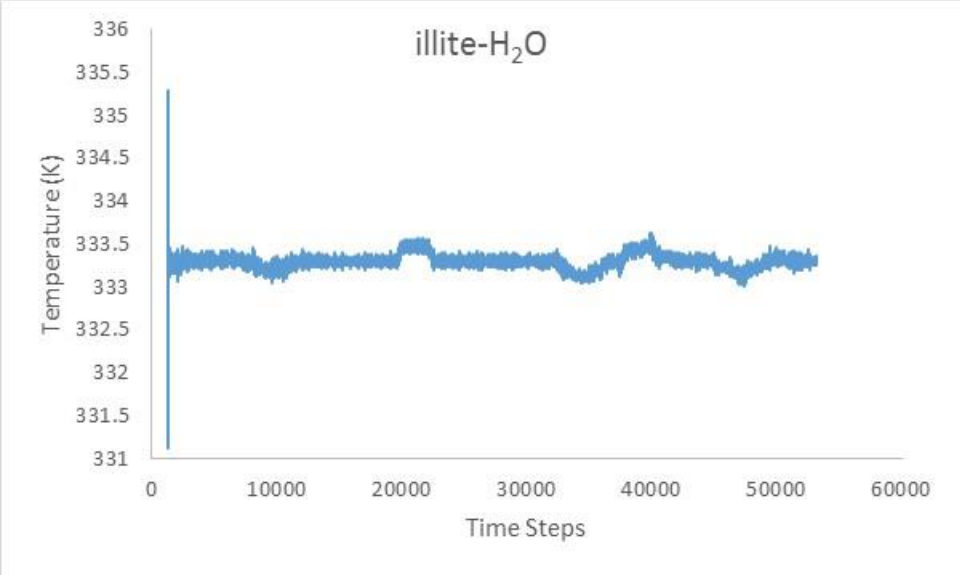

Temperature vs time steps for MD simulations

Illite-0K^+-PMMA with CO_2 in pore space-MD

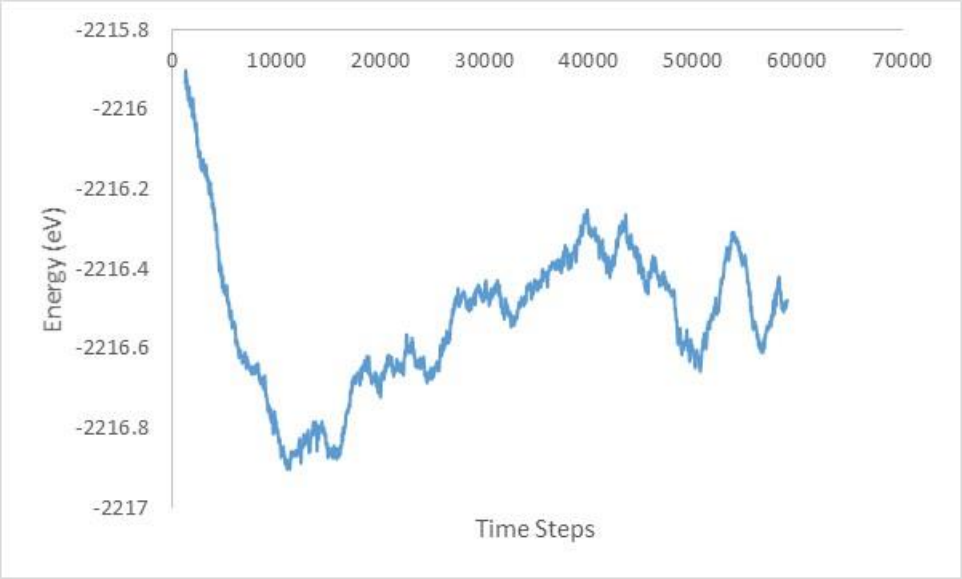

Energy vs time steps for MD simulations

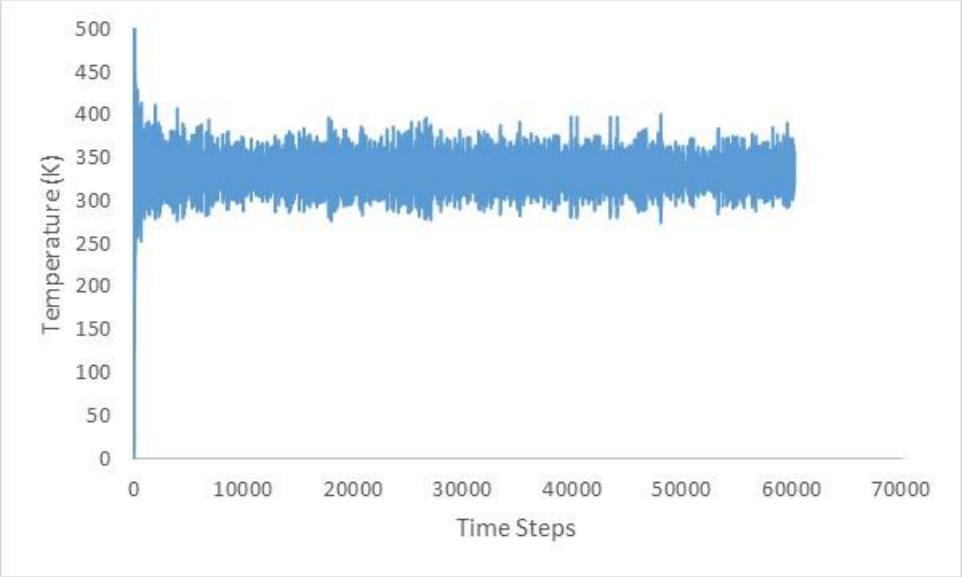

Temperature vs time steps for MD simulations